© 2014. Published by The Company of Biologists Ltd | Development (2014) 141, 4320-4331 doi:10.1242/dev.115022

RESEARCH ARTICLE

TBX1 regulates epithelial polarity and dynamic basal filopodia in the second heart field

Alexandre Francou, Edouard Saint-Michel, Karim Mesbah and Robert G. Kelly*

ABSTRACT

Elongation of the vertebrate heart occurs by progressive addition of second heart field (SHF) cardiac progenitor cells from pharyngeal mesoderm to the poles of the heart tube. The importance of these cells in the etiology of congenital heart defects has led to extensive research into the regulation of SHF deployment by signaling pathways and transcription factors. However, the basic cellular features of these progenitor cells, including epithelial polarity, cell shape and cell dynamics, remain poorly characterized. Here, using immunofluorescence, live imaging and embryo culture, we demonstrate that SHF cells constitute an atypical, apicobasally polarized epithelium in the dorsal pericardial wall, characterized by apical monocilia and dynamic actin-rich basal filopodia. We identify the 22q11.2 deletion syndrome gene *Tbx1*, required in the SHF for outflow tract development, as a regulator of the epithelial properties of SHF cells. Cell shape changes in mutant embryos include increased circularity, a reduced basolateral membrane domain and impaired filopodial activity, and are associated with elevated aPKCζ levels. Activation of aPKCζ in embryo culture similarly impairs filopodia activity and phenocopies proliferative defects and ectopic differentiation observed in the SHF of *Tbx1* null embryos. Our results reveal that epithelial and progenitor cell status are coupled in the SHF, identifying control of cell shape as a regulatory step in heart tube elongation and outflow tract morphogenesis.

KEY WORDS: Cardiac progenitor cells, Apicobasal polarity, TBX1, Mouse

INTRODUCTION

Morphogenesis of the embryonic heart occurs by addition of cardiac progenitor cells to the elongating arterial and venous poles of the heart tube (Cai et al., 2003; Kelly et al., 2001; Mjaatvedt et al., 2001; Waldo et al., 2001). These progenitor cells, termed the second heart field (SHF), are located in splanchnic mesoderm in the dorsal wall of the coelomic or pericardial cavity (dorsal pericardial wall, DPW) and are characterized by elevated proliferation and delayed differentiation (Kelly, 2012; Vincent and Buckingham, 2010). Anterior and posterior SHF populations have been identified that contribute to the right ventricle and outflow tract (OFT) at the arterial pole and atrial myocardium at the venous pole, respectively (Vincent and Buckingham, 2010). Perturbation of SHF development results in a shorter heart tube that fails to remodel correctly during cardiac septation, leading to a spectrum of morphological anomalies (Dyer and Kirby, 2009). Understanding how progressive deployment of SHF cells is regulated is therefore an important step towards deciphering the origins of congenital heart defects. Previous research has focused on the signaling pathways and transcription factors operating in the SHF, including the LIM homeodomain transcription factor Isl1, required for heart tube elongation, and the T-box-containing transcription factor TBX1, required for development of the distal OFT (Cai et al., 2003; Dyer and Kirby, 2009; Xu et al., 2004). *TBX1* regulates proliferation and differentiation in the SHF and is the major gene implicated in 22q11.2 deletion (or DiGeorge) syndrome, a primary cause of congenital heart defects affecting the cardiac OFT (Chen et al., 2009; Liao et al., 2008; Pane et al., 2012; Papangeli and Scambler, 2013). However, despite progress in dissecting SHF regulatory networks, basic cellular features of the SHF, including cell polarity, cell shape and cell dynamics, remain to be investigated.

Polarized epithelia play central roles in embryonic development. In particular, the formation and remodeling of epithelia drive diverse morphogenetic processes, and reiterative rounds of mesenchymal-to-epithelial and epithelial-to-mesenchymal transitions accompany organogenesis, including heart development (Thiery et al., 2009). In the early embryo, cardiac progenitor cells, giving rise to the cardiac crescent and linear heart tube, are located in anterior splanchnic mesoderm and form an epithelial sheet in the ventral midline. The epithelial properties of these early cardiac cells have been studied by Linask and colleagues in the avian embryo, where epithelialization and the regulation of N-Cadherin accumulation has been shown to play an important role in the onset of differentiation (Linask, 1992; Linask et al., 2005). The epithelial organization of myocardial cells has also been studied in zebrafish, where basal accumulation of fibronectin, regulated by Hand2, and the polarized epithelial organization of myocardial cells downstream of Has/PKCι are required for normal morphogenesis of the early fish heart (Rohr et al., 2006; Trinh and Stainier, 2004; Trinh et al., 2005). By contrast, the epithelial properties of SHF cells located in the DPW during late stages of vertebrate heart tube elongation have received less attention. In a pioneering study, Virágh and Challice showed, using light and electron microscopy, that cells adjacent to the distal border of the heart tube of the mid-gestation mouse embryo form a cuboidal epithelium of condensed mesenchymal cells (Virágh and Challice, 1973). However, molecular characterization of the epithelial properties of SHF cells has not been performed and the regulators of such properties are unknown.

Here, we characterize apicobasal polarity, cell shape and cell dynamics in the murine SHF. We demonstrate that SHF cells constitute an atypical polarized epithelium with apical monocilia and dynamic basal filopodia, visualized by time-lapse microscopy of living SHF cells. Furthermore, we show that TBX1 is a regulator of epithelial cell morphology in the DPW. Cell shape changes in mutant embryos include increased circularity, a reduced basolateral membrane domain and impaired filopodial activity, and are associated with elevated aPKCζ levels. Using embryo culture, we show that activation of aPKCζ similarly impairs filopodia activity and phenocopies proliferative defects and ectopic differentiation

Aix Marseille Université, CNRS, IBDM UMR 7288, Marseille 13288, France.

*Author for correspondence (Robert.Kelly@univ-amu.fr)

Received 3 July 2014; Accepted 15 September 2014

Development (2014) 141, 4320-4331 doi:10.1242/dev.115022

observed in the DPW of *Tbx1* null embryos. Our results identify control of the epithelial properties of SHF progenitor cells as a regulatory step in progressive heart tube elongation and OFT morphogenesis.

RESULTS

Cardiac progenitor cells in the dorsal pericardial wall constitute an apicobasally polarized epithelium

The mouse heart tube undergoes rapid elongation by addition of cardiac progenitor cells from the SHF between embryonic days (E) 8.5 and 10.5. At E9.5, SHF cells expressing an *Fgf10* enhancer trap transgene (*Fgf10-nlacZ*) and Isl1 are located in splanchnic mesoderm in the DPW (Fig. 1A-D). We investigated the epithelial properties of SHF cells in the DPW using immunofluorescence microscopy (Fig. 1E-N). aPKCζ and Crumbs3 [crumbs homolog 3 (Drosophila), Crb3 – Mouse Genome Informatics] are localized at the apical membrane and are enriched at cell-cell junctions in the DPW (Fig. 1E,G,H); by contrast, Scribble is localized at the basolateral membrane (Fig. 1F,G). The tight junction protein ZO-1 (Tjp1 – Mouse Genome Informatics) accumulates at apical cell-cell junctions in the DPW (Fig. 1I) together with Par3 and PATJ (Inadl – Mouse Genome Informatics) (supplementary material Fig. S1). Adherens junctions are present at the boundary between apical (aPKCζ positive) and basolateral (Scribble positive) membrane domains, labeled by N-cadherin and, at lower levels, E-cadherin (Fig. 1J-L; supplementary material Fig. S1). Basally, SHF cells are characterized by an irregular basal lamina and a fibronectin-rich extracellular matrix (Fig. 1M,N). Together, these results demonstrate that *Fgf10-nlacZ*- and Isl1-expressing cells in the DPW constitute an apicobasally polarized epithelium, with an apical surface facing the pericardial cavity and a basal surface facing underlying mesenchyme and pharyngeal endoderm. These epithelial properties are shared with the columnar epithelium of the overlying pharyngeal endoderm, although the latter is distinguished by higher levels of E-cadherin accumulation and a more continuous basal lamina (Fig. 1E-N).

Spatial heterogeneity and maturation of epithelial cells in the dorsal pericardial wall

SHF cells contribute to the growth of the OFT at the arterial pole of the heart and to atrial myocardium at the venous pole, corresponding to anterior and posterior domains of the SHF (Vincent and Buckingham, 2010). Whereas Isl1 is expressed in both domains, *Fgf10-nlacZ* expression is restricted to the anterior region (Fig. 2A,B; Cai et al., 2003; Kelly et al., 2001). We investigated whether cells differ in their epithelial properties in the anterior (aDPW, *Fgf10-nlacZ* expressing) and posterior (pDPW, *Fgf10-nlacZ* non-expressing) DPW (Fig. 2). ZO-1 and aPKCζ/Scribble are expressed in Isl1-positive cells throughout the DPW (Fig. 2B; supplementary material Fig. S2). N-cadherin is also expressed in the entire DPW, although with a gradient increasing towards the venous pole, and is strongly expressed in differentiated cardiomyocytes (Fig. 2C,G; supplementary material Fig. S2). By contrast, E-cadherin accumulates only in the aDPW and the most lateral regions of the pDPW and is maintained in differentiated cardiomyocytes in the OFT (Fig. 2D,G; supplementary material Fig. S2). A basal lamina is not apparent in the pDPW, in contrast to the aDPW (Fig. 2E-E″; supplementary material Fig. S2), and a low level of fibronectin labeling between cells was observed in the pDPW (Fig. 2F-F″; supplementary material Fig. S2). The pDPW is thus a distinct epithelial domain within the DPW, with elevated N-cadherin levels, lack of E-cadherin and a reduced basal lamina.

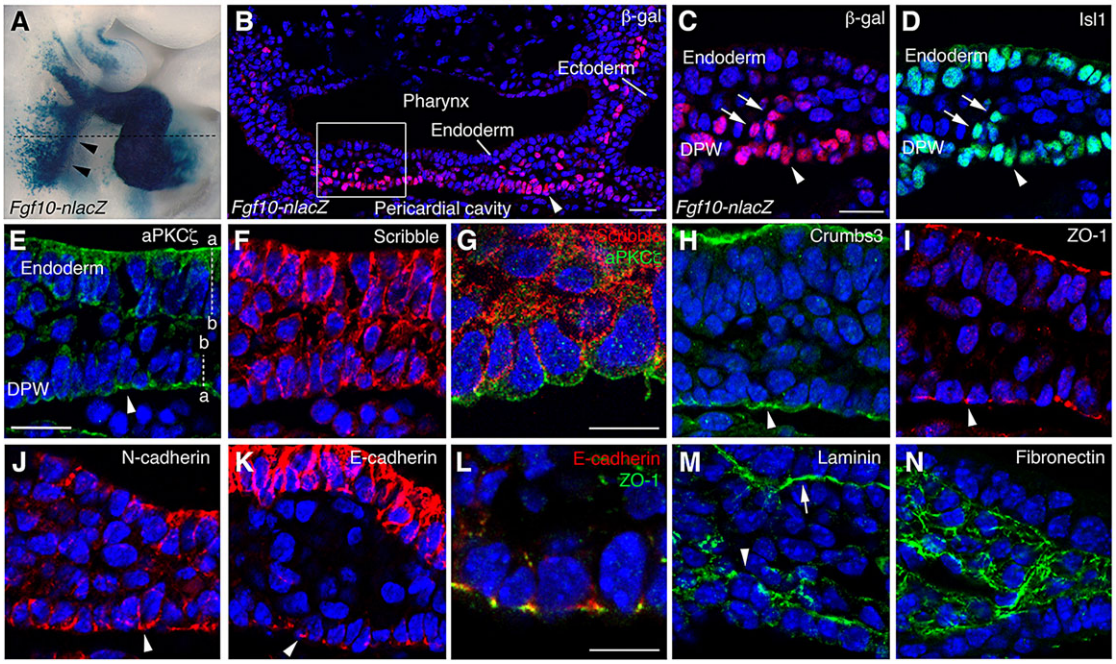

Fig. 1. Cardiac progenitor cells in the dorsal pericardial wall constitute a polarized epithelium. (A) *Fgf10-nlacZ* transgene expression in the arterial pole of the heart and pharyngeal mesoderm (arrowheads) at E9.5. (B-N) Immunofluorescence on transverse sections at the level of the dashed line in A. (B-D) Distribution of *Fgf10-nlacZ*- and Isl1-expressing cells in the DPW (arrowheads) and overlying mesenchyme (arrows), the region shown in C-N is boxed in B. (E-H) aPKCζ and Crumbs3 accumulate in the apical membrane and junctions, and Scribble in the basolateral membrane of DPW cells (arrowheads). (G) High-magnification view showing complementary membrane domains identified by Scribble and aPKCζ. (I) ZO-1 accumulates apically at cell junctions (arrowhead). (J) N-cadherin accumulates predominantly on the apical side (arrowhead). (K) E-cadherin accumulates apically, close to sites of ZO-1 labeling shown in L. (M) Laminin forms an irregular basal lamina with gaps in the DPW (arrowhead). Note the organized endodermal basal lamina (arrow). (N) Fibronectin accumulates in the mesenchyme on the basal side of the DPW. Dashed lines in E indicate the apicobasal axis of the DPW and endodermal epithelia. a, apical; b, basal. Scale bars: B: 30 µm; C-F,H-K,M,N: 20 µm; G,L: 10 µm.

Development (2014) 141, 4320-4331 doi:10.1242/dev.115022

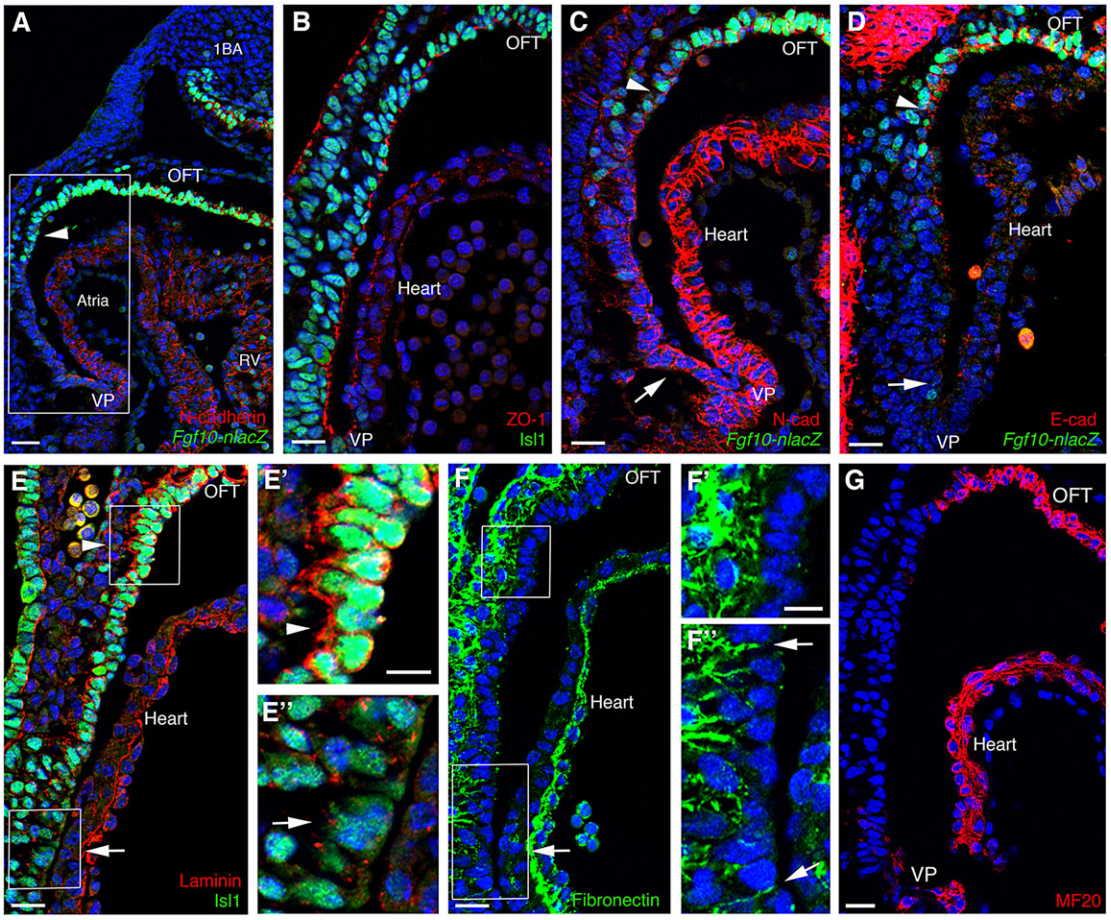

Fig. 2. Spatial heterogeneity of epithelial properties in the dorsal pericardial wall. Sagittal sections at E9.5 showing (A) the distribution of *Fgf10-nlacZ*-expressing cells in the OFT and aDPW (arrowhead); the region shown in B-G is boxed in A. (B) ZO-1 is observed throughout the ISL1-positive DPW. (C) N-cadherin is expressed in the entire DPW (aDPW, arrowhead), with a gradient increasing towards the inflow (pDPW, arrow). (D) E-cadherin accumulates in the aDPW (arrowhead) and in the OFT, but not in the pDPW (arrow). (E-E″) Laminin accumulates predominantly in the aDPW (arrowheads), with only puncti observed in the pDPW (arrows). The regions shown in E′,E″ are boxed in E. (F-F″) Fibronectin is observed on the basal side of cells in the aDPW (F,F′) and occasionally between cells in the pDPW (arrows). The regions shown in F′,F″ are boxed in F. (G) Sarcomeric myosin heavy chain expression in differentiated myocardium detected by the anti-MF20 antibody. 1BA, first branchial arch; OFT, outflow tract; RV, right ventricle; VP, venous pole. Scale bars: A: 30 µm; B-E,F,G: 20 µm; E′,E″,F′,F″: 10 µm.

A day earlier in development, at E8.5, the distribution of ZO-1, aPKCζ, Scribble and N-cadherin accumulation in the DPW is similar to that at E9.5 (supplementary material Fig. S3). However, the DPW is entirely E-cadherin negative and the basal lamina is not well formed, as indicated by punctuated laminin staining (supplementary material Fig. S3). Cells in the coelomic wall are apicobasally polarized as early as E7.5, although N-cadherin expression is less apically enriched and a basal lamina is absent (supplementary material Fig. S3). This spatiotemporal heterogeneity suggests that the epithelial properties of the DPW progressively mature and diversify as SHF cells contribute to the cardiac poles, with the appearance of E-cadherin-containing junctions and a basal lamina in the aDPW by E9.5. Such differential epithelial properties might underlie segregation of anterior and posterior progenitor cell populations during SHF deployment.

Cells in the dorsal pericardial wall form dynamic basal filopodia

The epithelial structure of DPW cells was further investigated by transmission electron microscopy (TEM) at E8.5 and E9.5. DPW cells are characterized by an elongated triangular shape with a smooth convex apical surface (Fig. 3A). Cell contacts are restricted to the apical region, where tight and adherens junction proteins accumulate (Fig. 3A,B, arrows). Scanning EM and immunofluorescence with an anti-acetylated-α-tubulin antibody revealed that the smooth apical surface is characterized by the presence of monocilia with a 9+0 microtubule structure, extending into the pericardial cavity (Fig. 3D,E). The basolateral membrane of epithelial cells in the DPW was observed to form multiple filopodia-like protrusions, which are more commonly observed in mesenchymal cells (Fig. 3A, arrowhead). The shape and organization of epithelial cells in the DPW, in particular the presence of such basolateral protrusions, thus differs significantly from those of columnar epithelia such as pharyngeal endoderm (Fig. 3C). Visualization of basal protrusions was facilitated by *Mesp1-Cre* activation of a conditional *GFP* reporter gene (Fig. 3F,G). Together with TEM and phalloidin staining on sagittal and transverse sections, these data revealed that basal filopodia are present throughout the DPW (supplementary material Fig. S4). Furthermore, these protrusions are enriched in actin filaments and microtubules, confirming their identification as filopodia-like structures (Fig. 3H,I).

In order to investigate the dynamic properties and contacts of these filopodia-like structures, we established a thick-slice culture protocol and performed live-imaging of cells in the DPW. Time-lapse microscopy of transverse slices from E8.5 and E9.5 embryos, using the *Mesp1-Cre* activated GFP reporter, allowed the first visualization of

Development (2014) 141, 4320-4331 doi:10.1242/dev.115022

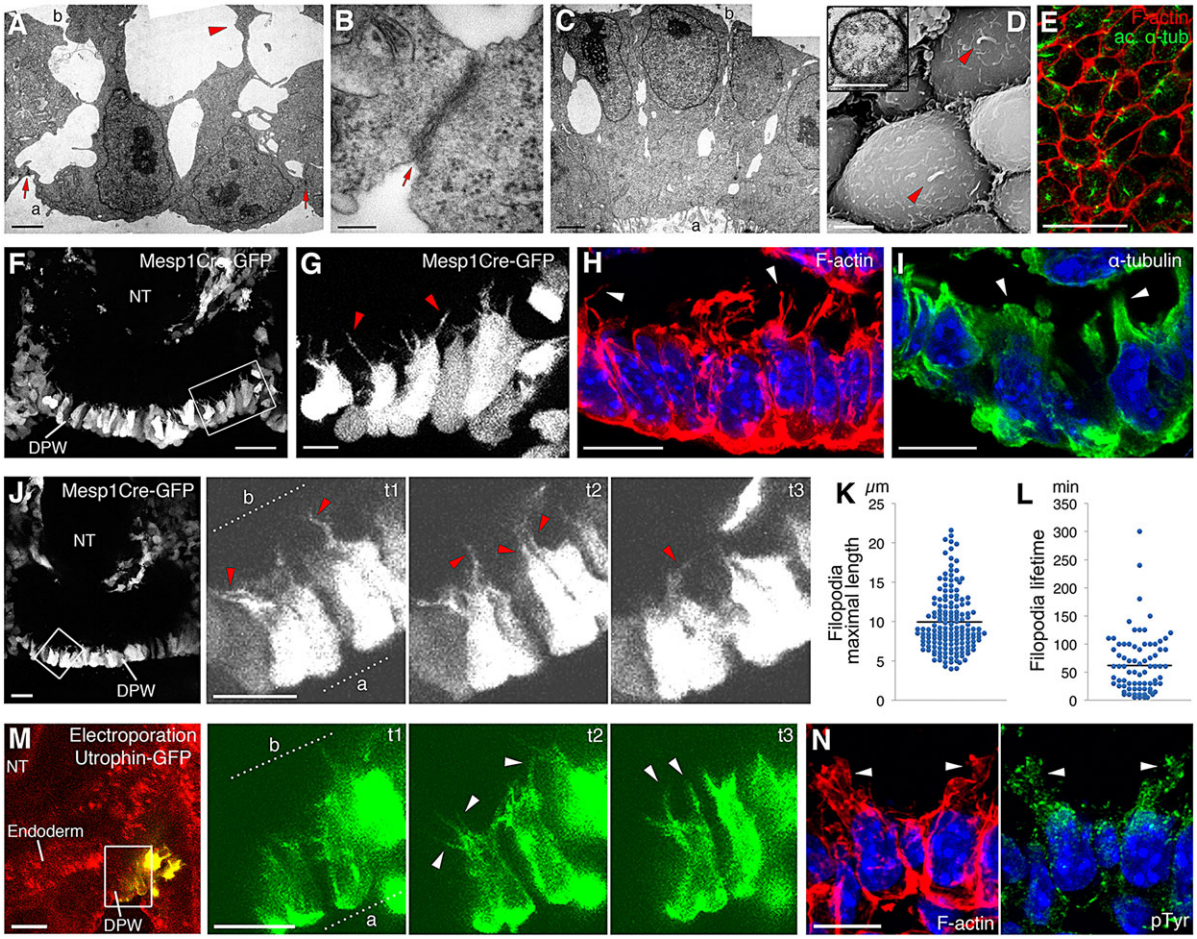

Fig. 3. Epithelial cells in the dorsal pericardial wall form dynamic basal filopodia. (A) TEM showing the atypical triangular shape of DPW cells with apical cell junctions (a, arrows) and basal protrusions (arrowhead). (B) High magnification showing apical junctional complexes (arrow). (C) Transmission electron micrograph of pharyngeal endodermal epithelium. (D) Ventral scanning electron micrograph of an E9.5 wild-type embryo, showing the apical surface of DPW cells with apical primary cilia (red arrowheads) with 9+0 microtubule structure (TEM, inset box). (E) Whole-mount immunolabeling of acetylated α-tubulin, showing apical primary cilia (green). (F) Transverse slice showing expression of a *Mesp1Cre*-activated *GFP* reporter gene at E8.5. (G) GFP-positive cells from the boxed region in F, showing extensive basal protrusions (red arrowheads). (H,I) Actin filaments and microtubules accumulate in the basal filopodia (white arrowheads). (J) Snapshot of a transverse slice of a *Mesp1Cre*;*Z/EG* E8.5 embryo, and three time-points extracted from a time-lapse movie showing dynamic basal filopodia (red arrowheads). (K,L) Distribution of maximal filopodial length (K, *n*=158 cells from 13 embryos) and lifetime (L, *n*=80 cells from 12 embryos). (M) Transverse slice of an E8.5 embryo electroporated with *Utrophin-GFP*, and three time-points showing dynamic basal actin filaments (white arrowheads). (N) High magnification of a transverse section at E9.5, showing subcellular accumulation of phospho-tyrosine F-actin-containing in basal filopodia (white arrowheads). a, apical; b, basal. Scale bars: E,F: 20 μm; A,C,D: 2 μm; B,D inset: 200 nm, G-J,M,N: 10 μm.

cell behavior in the SHF. These experiments revealed that the basal filopodia are highly dynamic, extending towards and making contact with overlying mesenchyme and pharyngeal endoderm (Fig. 3J; supplementary material Fig. S5 and Movie 1). Quantification of filopodial parameters revealed that basal DPW filopodia extend from 4 μm to 22 μm (Fig. 3K) and have a lifetime ranging from a single timeframe (5 min or less) to 300 min, with a mean duration of 62 min (Fig. 3L). In order to visualize actin filament dynamics, a plasmid encoding an utrophin-GFP fusion protein, which binds F-actin without disturbing actin assembly or disassembly (Burkel et al., 2007), was electroporated into the DPW (Fig. 4M). Time-lapse microscopy of electroporated cells revealed that actin accumulated apically and in the basal protrusions, where dynamic extension and retraction of actin filaments was observed (Fig. 3M; supplementary material Movie 2, left), suggesting that DPW filopodial movement is driven by active actin filament remodeling. Multiple intercellular signaling pathways have been shown to regulate SHF development, including fibroblast growth factor (FGF) signaling that promotes proliferation in the SHF (reviewed by Rochais et al., 2009). We investigated whether basal filopodia could sense FGF signaling, using an anti-phospho-tyrosine (p-Tyr) antibody to score subcellular localization of receptor activation. In support of a sensing role, p-Tyr staining accumulates in the basal filopodia of DPW cells (Fig. 3N).

TBX1 is required for normal SHF cell shape and apicobasal polarity

The 22q11.2 deletion syndrome candidate gene *Tbx1* encodes a key regulator of pharyngeal morphogenesis and SHF development (Chen et al., 2009; Liao et al., 2008). We investigated whether altered epithelial properties are associated with abnormal SHF development in $Tbx1^{-/-}$ embryos. Although SHF cells in $Tbx1^{-/-}$ embryos are apicobasally polarized, they appear rounder than cells in control embryos (Fig. 4). Quantification of the circularity index, using aPKCζ and Scribble to visualize cell membranes, confirmed that SHF cells are significantly rounder in the aDPW of $Tbx1^{-/-}$ than in wild-type embryos (Fig. 4A-G). Further analysis revealed that cells in the $Tbx1^{-/-}$ aDPW have expanded apical (aPKCζ positive) and reduced basolateral (Scribble positive) membrane domains and

Development (2014) 141, 4320-4331 doi:10.1242/dev.115022

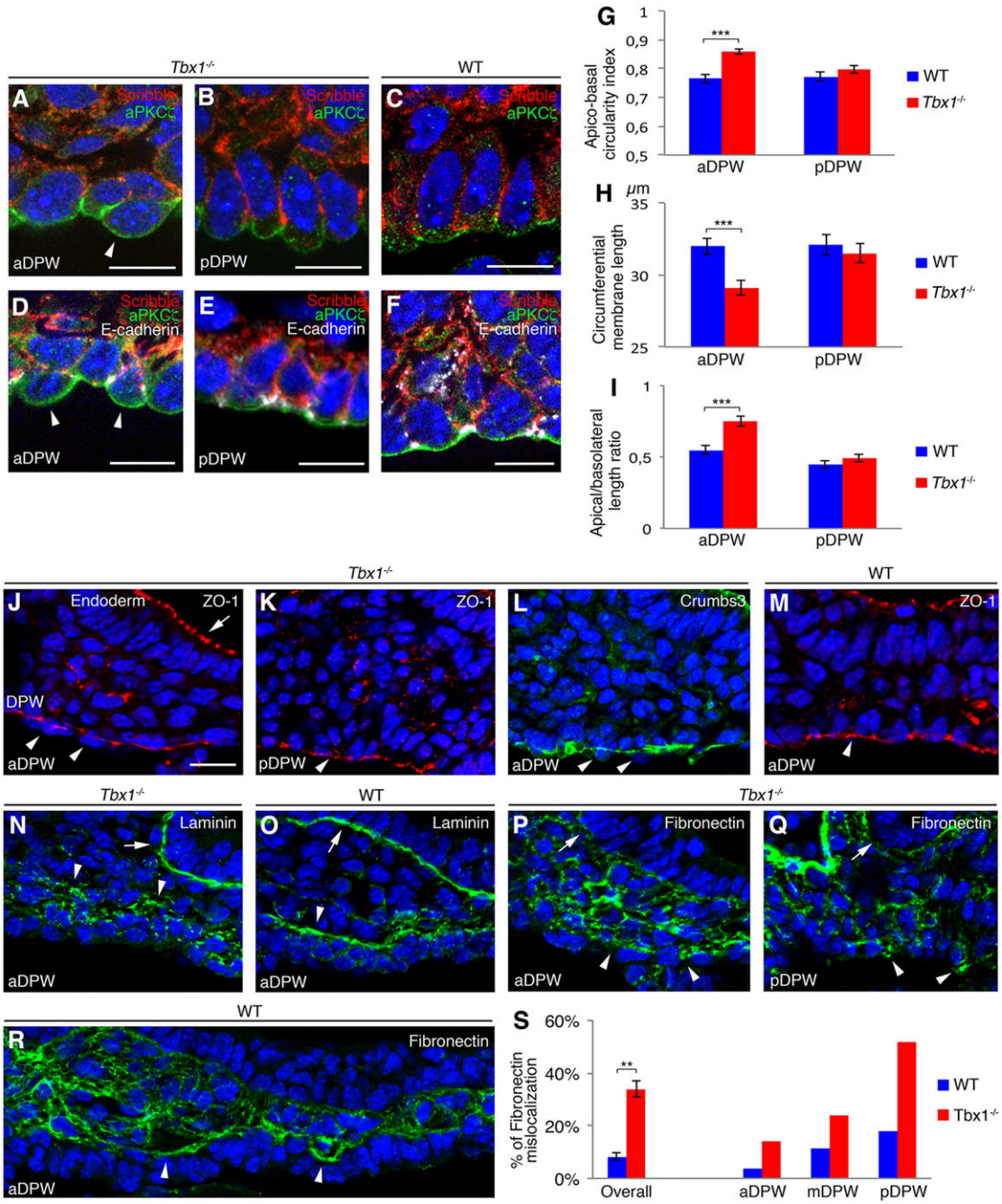

Fig. 4. TBX1 regulates cell shape, apical-basolateral membrane domains and epithelial organization in the anterior DPW. Immunofluorescence of aPKCζ and Scribble staining in *Tbx1*$^{-/-}$ embryos reveals rounded cells in the aDPW (A, arrowhead) and normally elongated cells in the pDPW (B) compared with wild type (C). (D) aPKCζ, Scribble and E-cadherin staining in the *Tbx1*$^{-/-}$ aDPW showing expanded apical and reduced basolateral membrane domains (arrowheads), separated by E-cadherin-positive junctions (white) compared with the pDPW (E) and wild-type (F) situations. (G) Quantification of the apicobasal circularity index. (H,I) Membrane length measurements show a reduction of circumferential membrane length (H) and increased apical/basolateral membrane ratio (I) in the *Tbx1*$^{-/-}$ aDPW (n=185 cells from three wild-type embryos, 260 cells from three *Tbx1*$^{-/-}$ embryos). (J-L) ZO-1 (J,K) and Crumbs3 (L) are abnormally localized on the basal side of extruded nuclei in the aDPW of *Tbx1*$^{-/-}$ embryos (arrowheads), but are normally localized in the endoderm (J, arrow) and pDPW (K, arrowhead), as in wild type (M). (N) Laminin is more punctuated and diffuse (arrowheads) in the aDPW of *Tbx1*$^{-/-}$ embryos but is normal in endoderm (arrow) compared with wild type (O). (P,Q) More fibronectin labeling is observed between epithelial cells (arrowheads) in the aDPW (P) and pDPW (Q) compared with wild type (WT) (R). (S) Quantification showing the incidence of fibronectin mislocalization throughout the DPW (left) and in three regions of wild type versus *Tbx1*$^{-/-}$ embryos (aDPW, anterior; mDPW, middle; pDPW, posterior) (n=1242 cells from six wild-type embryos, 897 cells from six *Tbx1*$^{-/-}$ embryos). $^{**}P$<0.01; $^{***}P$<0.001. Error bars in G,H,I,S represent s.e.m. Scale bars: A-F: 10 μm; J-R: 20 μm.

that cells are partially extruded from the epithelium (Fig. 4A,D; supplementary material Movie 3). Extruded cells with enlarged apical domains were also observed using TEM (Fig. 5F). E-cadherin labeling revealed that the interface between apical and basolateral domains is shifted basally (Fig. 4D-F). Quantification revealed that total circumferential membrane length is reduced, whereas the apical/basolateral membrane ratio is increased in *Tbx1*$^{-/-}$ DPW cells (Fig. 4H,I). E- and N-cadherin, ZO-1 and Crumbs3 accumulate in the

Development (2014) 141, 4320-4331 doi:10.1242/dev.115022

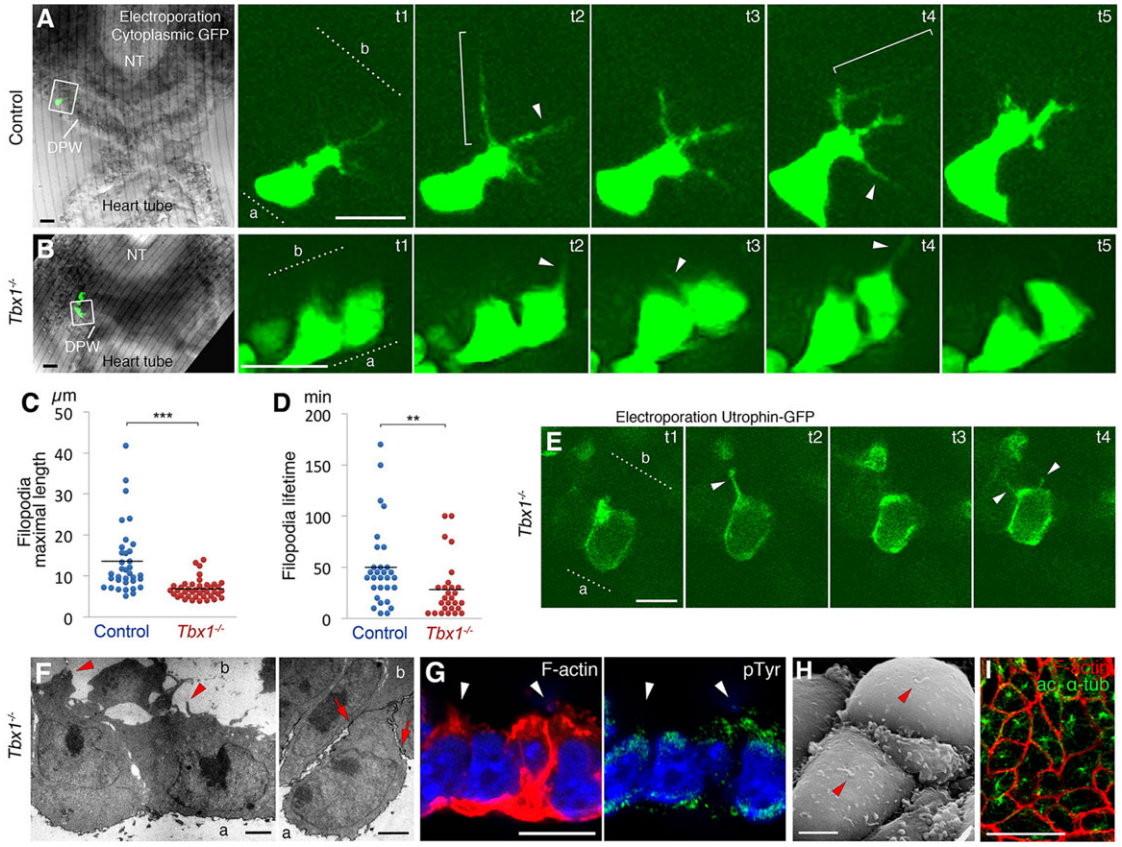

Fig. 5. Basal filopodial activity is impaired in the absence of TBX1. (A) Transverse slice of an E8.5 control embryo electroporated with a plasmid expressing cytoplasmic GFP, and a time-point series showing dynamic basal filopodia (arrowheads and brackets). (B) Time-point series of an E8.5 *Tbx1*$^{-/-}$ embryo after electroporation, showing shorter, less dynamic basal filopodia. (C) Measurement of maximal filopodial length in *GFP*-electroporated cells (n=35 cells from four control embryos, 41 cells from four *Tbx1*$^{-/-}$ embryos). (D) Measurement of filopodial lifetime (n=30 cells from four control embryos, 27 cells from four *Tbx1*$^{-/-}$ embryos). (E) Time-lapse imaging of an E8.5 *Tbx1*$^{-/-}$ embryo electroporated with *utrophin-GFP* (compare with Fig. 4N). (F) TEM showing rounder cells with fewer and smaller basal protrusions (red arrowheads), and enlarged apical membranes (red arrows show the junctions separating apical and basolateral domains). (G) Phalloidin staining showing reduced basal actin filaments and reduced phospho-tyrosine accumulation in residual filopodia (white arrowheads). (H,I) Scanning EM and immunolabeling show no defect in the formation and position of apical primary cilia (red arrowhead in H) in *Tbx1*$^{-/-}$ embryos. a, apical; b, basal. **P<0.01; ***P<0.001. Error bars in C,D represent s.e.m. Scale bars: A,B,I: 20 μm; E,G: 10 μm; F,H: 2 μm.

aDPW of *Tbx1*$^{-/-}$ mutant embryos with levels indistinguishable from those in wild-type embryos (Fig. 4J,L; data not shown). However, extruded cell nuclei can be observed on the pericardial side of these apical and junctional markers (Fig. 4J,L, arrowheads; supplementary material Movie 4), a situation not observed in wild-type embryos (Fig. 4M, arrowheads; supplementary material Movie 4), and consistent with a shifted interface between apical and basolateral domains. These phenotypes are restricted to anterior SHF progenitor cells in the aDPW, which is hypoplastic in *Tbx1*$^{-/-}$ embryos (Kelly and Papaioannou, 2007; Liao et al., 2008); close to the venous pole, epithelial organization is similar to that in wild-type embryos (Fig. 4). In addition to the changes described above, laminin staining is more punctuated and diffuse in the aDPW of *Tbx1*$^{-/-}$ embryos compared with wild-type embryos (Fig. 4N,O), suggesting defects in basal lamina establishment. Finally, increased localization of fibronectin between epithelial cells was observed throughout the *Tbx1*$^{-/-}$ DPW (Fig. 4P-S; supplementary material Movie 5). Together, these findings reveal that TBX1 regulates apicobasal polar properties and is required for normal cell shape in the aDPW.

Loss of TBX1 leads to impaired basal filopodial activity in dorsal pericardial wall cells

A reduction in the basal membrane of cells in the aDPW of *Tbx1*$^{-/-}$ embryos could impact on basal filopodia formation. We therefore investigated the dynamic properties of epithelial cells in *Tbx1*$^{-/-}$ embryos, using time-lapse imaging of slice cultures. Individual or small groups of cells were labeled by electroporation of a *CMV-GFP* plasmid into the DPW. Strong cytoplasmic GFP expression allowed visualization of long dynamic basal filopodia in control embryos at E8.5 (Fig. 5A; supplementary material Movie 6). At this stage, prior to overt morphological anomalies, *Tbx1*$^{-/-}$ embryos present a similar, although milder, epithelial phenotype to that in the aDPW at E9.5 (supplementary material Fig. S6). Cells in the DPW of *Tbx1*$^{-/-}$ embryos are rounder and form fewer and smaller filopodia (Fig. 5B; supplementary material Movie 6). Measurements of electroporated cells revealed that filopodia in control embryos extend from 5 μm to 42 μm, with a mean length of 13.5 μm (Fig. 5C). By contrast, significantly smaller filopodia were observed in *Tbx1*$^{-/-}$ embryos, extending from 4 μm to 14 μm, with a mean length of 7 μm (Fig. 5C). The lifetime of individual filopodia was also reduced in the absence of TBX1 (Fig. 5D). Utrophin-GFP was used to investigate actin filament dynamics, and rounder cells were observed in *Tbx1*$^{-/-}$ embryos, with fewer and smaller dynamic actin filaments on the basal side (Fig. 5E; supplementary material Movie 2). TEM revealed a similar filopodial phenotype in the *Tbx1*$^{-/-}$ aDPW at E9.5 (Fig. 5F). Basal actin filaments are reduced compared with wild type, and the residual filopodia show reduced p-Tyr labeling (Fig. 5G). By contrast, pDPW cells close to the venous pole of *Tbx1*$^{-/-}$ embryos maintain an

Development (2014) 141, 4320-4331 doi:10.1242/dev.115022

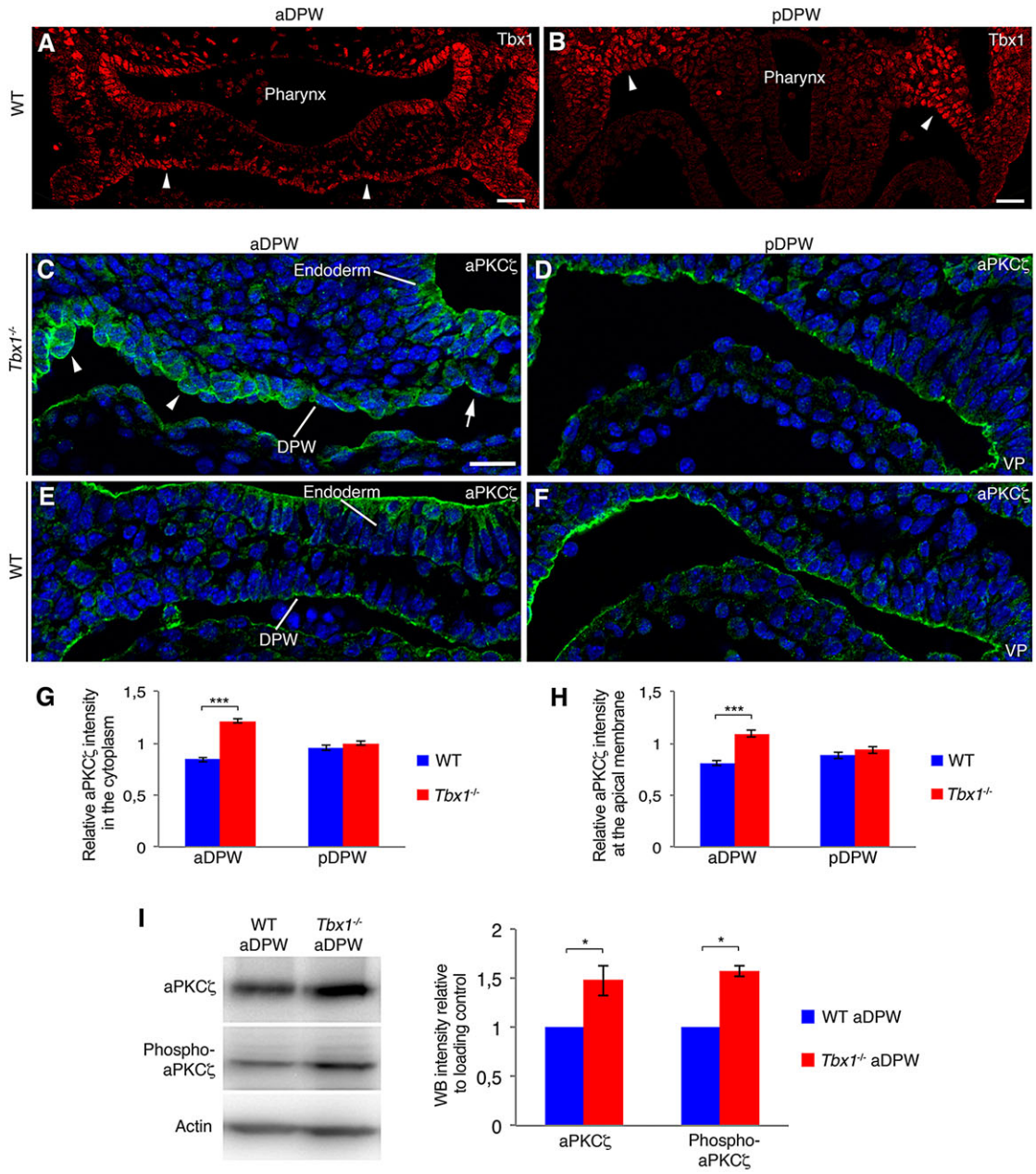

Fig. 6. Elevated aPKCζ protein levels in the dorsal pericardial wall of *Tbx1*$^{-/-}$ embryos. Transverse sections through the aDPW and pDPW of E9.5 wild-type and *Tbx1*$^{-/-}$ embryos. TBX1 is expressed in the aDPW (A, arrowheads), but in only in the most lateral cells of the pDPW (B, arrowheads). (C,D) Immunolabeling of aPKCζ, showing increased intensity of staining and rounded cells protruding apically (arrowheads) in the aDPW, but not in pDPW of *Tbx1*$^{-/-}$ embryos compared with wild type (E,F). (G,H) Quantification of aPKCζ labeling in the aDPW and pDPW in cytoplasmic (G; *n*=122 cells from three wild-type embryos, 202 cells from three *Tbx1*$^{-/-}$ embryos) and apical membrane (H; *n*=187 cells from three wild-type embryos, 274 cells from three *Tbx1*$^{-/-}$ embryos) compartments. (I) Western blot of microdissected aDPW and quantification of three western blots, showing increased aPKCζ and phosphorylated aPKCζ in *Tbx1*$^{-/-}$ embryos. **P*<0.05; ****P*<0.001. Error bars in G,H,I represent s.e.m. Scale bars: A-F: 20 µm.

elongated triangular shape with actin-enriched basal filopodia at E9.5 (supplementary material Fig. S6). Investigation of monocilia, using scanning EM and immunofluorescence, revealed that apically localized primary cilia are present throughout the *Tbx1*$^{-/-}$ DPW (Fig. 5H,I).

aPKCζ is upregulated in the dorsal pericardial wall of *Tbx1*$^{-/-}$ embryos

The observation that altered epithelial properties of the DPW in *Tbx1*$^{-/-}$ embryos are restricted to the aDPW is consistent with the expression of TBX1 in the aDPW and only the most lateral regions of the pDPW at E9.5 (Fig. 6A,B). Microarray analysis of *Tbx1*$^{-/-}$ embryos has identified a number of genes encoding epithelial proteins as potential TBX1 targets, including E-cadherin and Crumbs3 (Liao et al., 2008; van Bueren et al., 2010). However, the level of these two proteins appears to be unchanged in the aDPW of *Tbx1*$^{-/-}$ embryos (Fig. 5, and data not shown). By contrast, we observed increased intensity of aPKCζ immunolabeling in the aDPW of *Tbx1*$^{-/-}$ compared with wild-type embryos (Fig. 6C-F; supplementary material Fig. S7). This increase is particularly marked in lateral regions of the aDPW (Fig. 6C, arrowheads). aPKCζ is an important regulator of apicobasal polarity (Xiao and Liu, 2013). Indeed, aPKCζ

Development (2014) 141, 4320-4331 doi:10.1242/dev.115022

promotes the apical membrane domain of epithelial cells, and elevated aPKCζ levels might contribute to the reduction of the basolateral domain and impairment of basal filopodia in the *Tbx1*$^{-/-}$ DPW. We quantified the intensity of aPKCζ immunostaining, using high-magnification immunofluorescence in both the cytoplasm and apical cell membrane. The relative intensity of aPKCζ is significantly increased in both the cytoplasmic pool and at the apical membrane of *Tbx1*$^{-/-}$ aDPW cells (Fig. 6G,H), consistent with an increase in aPKCζ protein levels. By contrast, aPKCζ levels are comparable to wild type in adjacent mesenchymal cells, pharyngeal endoderm and the pDPW (Fig. 6, data not shown). Elevated aPKCζ expression is also observed in the most anterior region of the DPW in *Tbx1*$^{-/-}$ embryos at E8.5 (supplementary material Fig. S6). Increased aPKCζ levels in the DPW of *Tbx1*$^{-/-}$ embryos were confirmed by western blot; furthermore, these experiments revealed that the level of the active phosphorylated form of aPKCζ was increased in the pharyngeal region of *Tbx1*$^{-/-}$ embryos (Fig. 6I).

Activation of aPKCζ in embryo culture impairs filopodial activity and phenocopies proliferative defects and ectopic differentiation observed in *Tbx1* null embryos

In order to investigate the potential role of elevated aPKCζ levels in the etiology of the *Tbx1* null epithelial phenotype, we cultured E8.5 embryos for 24 h in the presence of a physiological activator of aPKCζ (El-Hashash et al., 2012; Limatola et al., 1994). Western blot analysis confirmed that the level of phosphorylated aPKCζ was increased after embryo culture (supplementary material Fig. S8). Investigation of the DPW in treated embryos revealed that apicobasal polarity is perturbed, associated with a significant reduction of the basal membrane (Fig. 7A-D). Strikingly, DPW cells in treated embryos form fewer basal filopodia compared with control embryos (Fig. 7E,F), similar to the situation in *Tbx1*$^{-/-}$ embryos. Given the potential role for DPW filopodia in environmental sensing and intercellular signal transmission, as suggested by localized p-Tyr expression, we investigated whether downstream signaling events in the FGF pathway were affected in treated embryos. Indeed, phospho-ERK staining is reduced in the DPW of treated, but not of control embryos, consistent with decreased FGF signaling and observations in *Tbx1*$^{-/-}$ embryos (Fig. 7G,H; supplementary material Fig. S8). FGF signaling plays an important pro-proliferative role in the SHF. We evaluated proliferation in the DPW of treated embryos and observed a significant reduction in the number of KI67 (Mki67 – Mouse Genome Informatics) and phosphorylated Histone H3 (PH3)-positive cells (Fig. 8A-D). TBX1 regulates both proliferation and differentiation in the SHF, and ectopic myocardial differentiation has been observed in the aDPW of *Tbx1*$^{-/-}$ embryos (Chen et al., 2009; Liao et al., 2008). We investigated whether altered epithelial properties in the DPW of embryos treated with the aPKCζ activator are associated with ectopic cell differentiation. In control embryos, sarcomeric myosin heavy chain (Myhc) is expressed in the distal OFT (Fig. 8E; supplementary material Fig. S8). In both *Tbx1*$^{-/-}$ and aPKCζ activator-treated embryos, differentiation is observed in the aDPW contiguous with the OFT (Fig. 8F-I; supplementary material Fig. S8). Quantification revealed elevated numbers of MF20-positive cells in the aDPW of aPKCζ activator-treated embryos compared with control embryos (Fig. 8F,H,I). Abnormal differentiation in the aDPW was confirmed with α-actinin, α-SMA and Troponin I (supplementary material Fig. S8), although differentiated cells in the aDPW continued to express the progenitor cell markers Isl1 and TBX1 (supplementary material Fig. S8). These results suggest that aPKCζ upregulation in *Tbx1*$^{-/-}$ embryos is unlikely to be a consequence of increased differentiation; furthermore, aPKCζ levels do not increase in differentiated OFT myocardium of wild-type embryos (supplementary material Fig. S7). Finally, we investigated whether the reduced proliferation and premature differentiation in the SHF of aPKCζ activator-treated embryos has an impact on OFT growth. Quantification of OFT morphology revealed that treated embryos have a significantly shorter and straighter OFT, with a larger angle between the distal and the proximal OFT compared with control embryos (Fig. 8J-L). Together, these results show that directly manipulating the epithelial properties of SHF progenitor cells by increasing activated aPKCζ levels leads to decreased proliferation and premature differentiation in the aDPW, and consequently to reduced extension of the myocardial OFT.

DISCUSSION

Cardiac progenitor cells giving rise to the linear heart tube differentiate within an N-cadherin-expressing epithelium in anterior lateral mesoderm (Linask, 1992; Linask et al., 2005). Our characterization of apicobasal polarity and cell morphology in the SHF reveals that these late differentiating progenitor cells retain epithelial status within an atypical polarized epithelium in the DPW. Furthermore, analysis of altered apicobasal polarity in the DPW of *Tbx1*$^{-/-}$ and aPKCζ activator-treated embryos implicates the control of epithelial properties of SHF cells as a regulatory step in progressive heart tube elongation and OFT morphogenesis.

SHF cells in the DPW have a triangular shape characterized by apical monocilia, and basal actin filament- and microtubule-enriched filopodia-like projections. Our investigation of the micro-behavior of living SHF cells demonstrates that the basal filopodia are highly dynamic. Cell protrusions have recently been reported in the caudal splanchnic mesoderm of mouse embryos, using phalloidin staining (Sinha et al., 2012). Although the dynamic properties of these protrusions were not examined, Sinha and colleagues suggested a potential involvement in cell intercalation, as mesenchymal SHF progenitors incorporate into a cohesive epithelial sheet prior to directional deployment towards the arterial pole. This model is consistent with our finding that the posterior SHF has a less developed basal lamina compared with the anterior SHF. Indeed, the epithelial properties of cardiac progenitor cells in the DPW progressively mature between E7.5 and E9.5 days of development as an E-cadherin- and laminin-positive aDPW domain is established. Such spatiotemporal heterogeneity might facilitate segregation of progenitor cells to the cardiac poles. Filopodia have been implicated in condensation and adhesion of colonization-competent cancer cells after extravasation (Shibue et al., 2012). However, we observed basal filopodia throughout the DPW epithelium, suggesting that their function is not limited to cell intercalation. Filopodia at the leading edge of migrating cells have been implicated in cell motility (Martín-Blanco and Knust, 2001); however, the basal localization of filopodia in DPW cells suggests that they are not involved in epithelial spreading. Filopodia have been recently implicated in environmental sensing, mediating, for example, Shh (Sanders et al., 2013), Notch (Cohen et al., 2010) or FGF signaling (Cooley et al., 2011). Proliferation and progressive differentiation of SHF cells is regulated by the concerted activity of multiple signaling pathways, including Hedgehog, Notch, FGF, BMP and canonical and non-canonical WNT signaling (Dyer and Kirby, 2009; Rochais et al., 2009). Filopodial extensions from the DPW directed to the overlying endoderm and adjacent mesenchymal cells might play a role in mediating signaling events required to maintain cardiac progenitor cell status in the DPW during heart

Development (2014) 141, 4320-4331 doi:10.1242/dev.115022

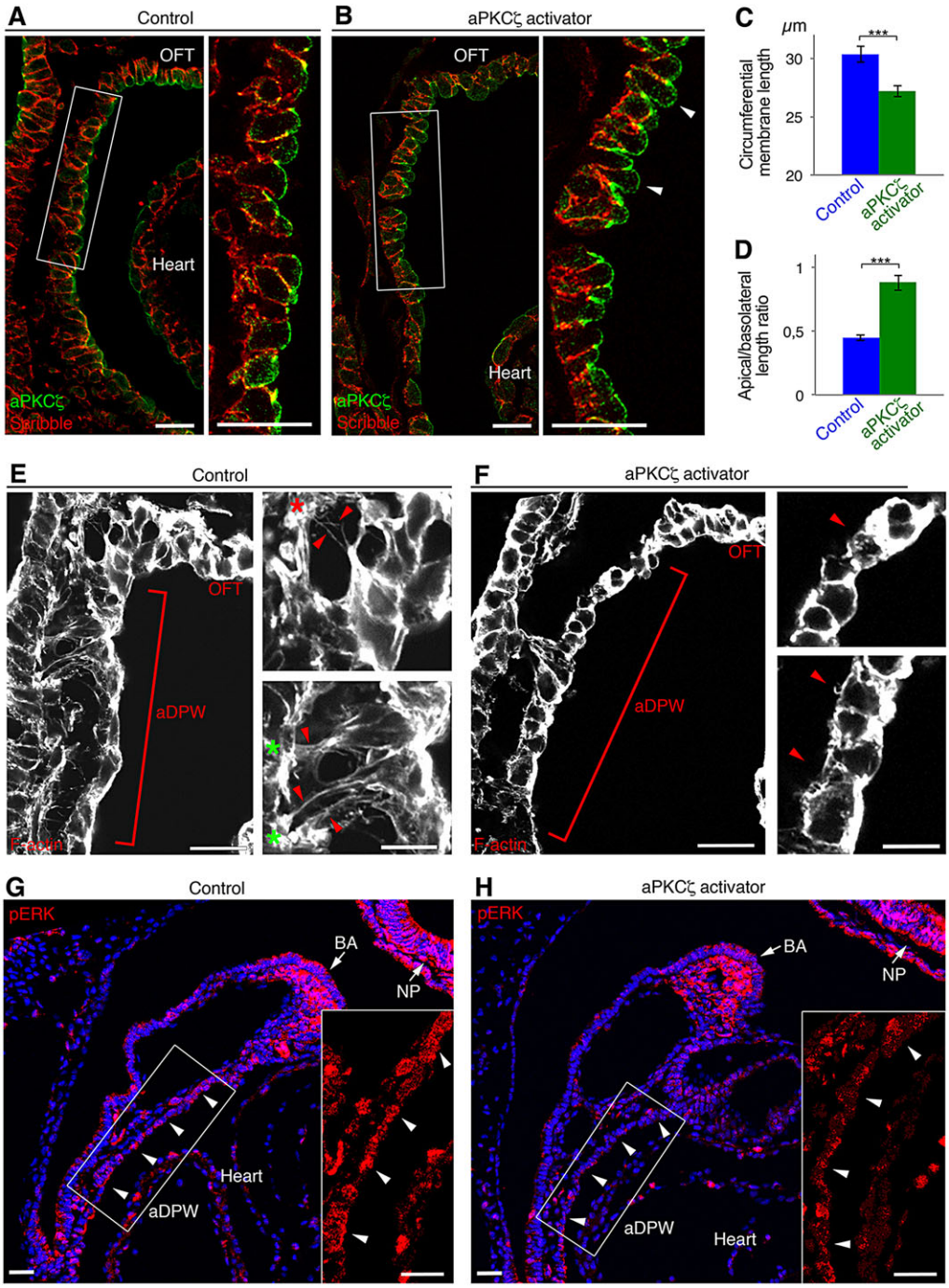

Fig. 7. Activation of aPKCζ perturbs apicobasal polarity and reduces basal filopodia formation and FGF signaling in the DPW. (A,B) Sagittal sections of control and aPKCζ activator-treated embryos, showing perturbed apicobasal polarity and enlarged apical membranes in DPW cells (B, arrowheads) compared with control; high-magnification views are boxed. (C,D) Quantification of total membrane length and apical/basolateral membrane length ratio for control and aPKCζ activator-treated embryos (*n*=65 cells from three control embryos, 108 cells from three treated embryos). (E,F) Sagittal sections of a control embryo, showing cells with multiple basal filopodia in the aDPW (E, arrowheads) and a treated embryo with reduced filopodia (F, arrowheads). Asterisks indicate mesenchymal (red) and endodermal (green) cells contacted by filopodia. (G,H) Sagittal sections showing decreased phospho-ERK labeling in the DPW of a treated embryo compared with a control embryo (arrowheads). Note that phospho-ERK labeling is unchanged in the first branchial arch (BA) and nasal pit (NP). Insets are high-magnification views of the boxed regions. ***P<0.001. Error bars in C,D represent s.e.m. Scale bars: E and F high-magnification insets: 10 μm; A,B,E,F: 20 μm; G,H: 30 μm.

tube extension. In support of a sensing role we observed elevated anti-phospho-tyrosine antibody staining in filopodia, consistent with FGF receptor activation. Furthermore, loss of filopodia in *Tbx1*$^{-/-}$ and aPKCζ activator-treated embryos is associated with decreased FGF signaling, reduced proliferation and ectopic differentiation in the SHF (Vitelli et al., 2002; Fig. 8).

TBX1 is required in pharyngeal mesoderm to regulate SHF proliferation and differentiation (Chen et al., 2009; Liao et al., 2008; Zhang et al., 2006). Our results show that TBX1 also regulates epithelial properties of SHF cells: in *Tbx1*$^{-/-}$ embryos aDPW cells are rounder, have expanded apical and decreased basolateral membrane domains, and form fewer filopodia with a shorter lifetime. Consequently, a fraction of DPW cells are partly extruded into the pericardial cavity. In addition to these changes, we observed that the basal lamina is disorganized in the absence of TBX1, with an elevated incidence of fibronectin mislocalization. Altered basal extracellular matrix properties might also impact on the formation and duration of filopodia. Increased circularity of cardiomyocytes in *tbx1* mutant zebrafish hearts has recently been reported (Choudhry and Trede, 2013). This appears to reflect a block in the transition from a rounded morphology in the early heart tube to an anisotropic elongated shape in the outer curvature of the fish heart. Our results provide further evidence of a role for TBX1 in regulating cell shape, and suggest that the regulation of epithelial status and basal filopodia are additional mechanisms by which TBX1 controls SHF development.

Development (2014) 141, 4320-4331 doi:10.1242/dev.115022

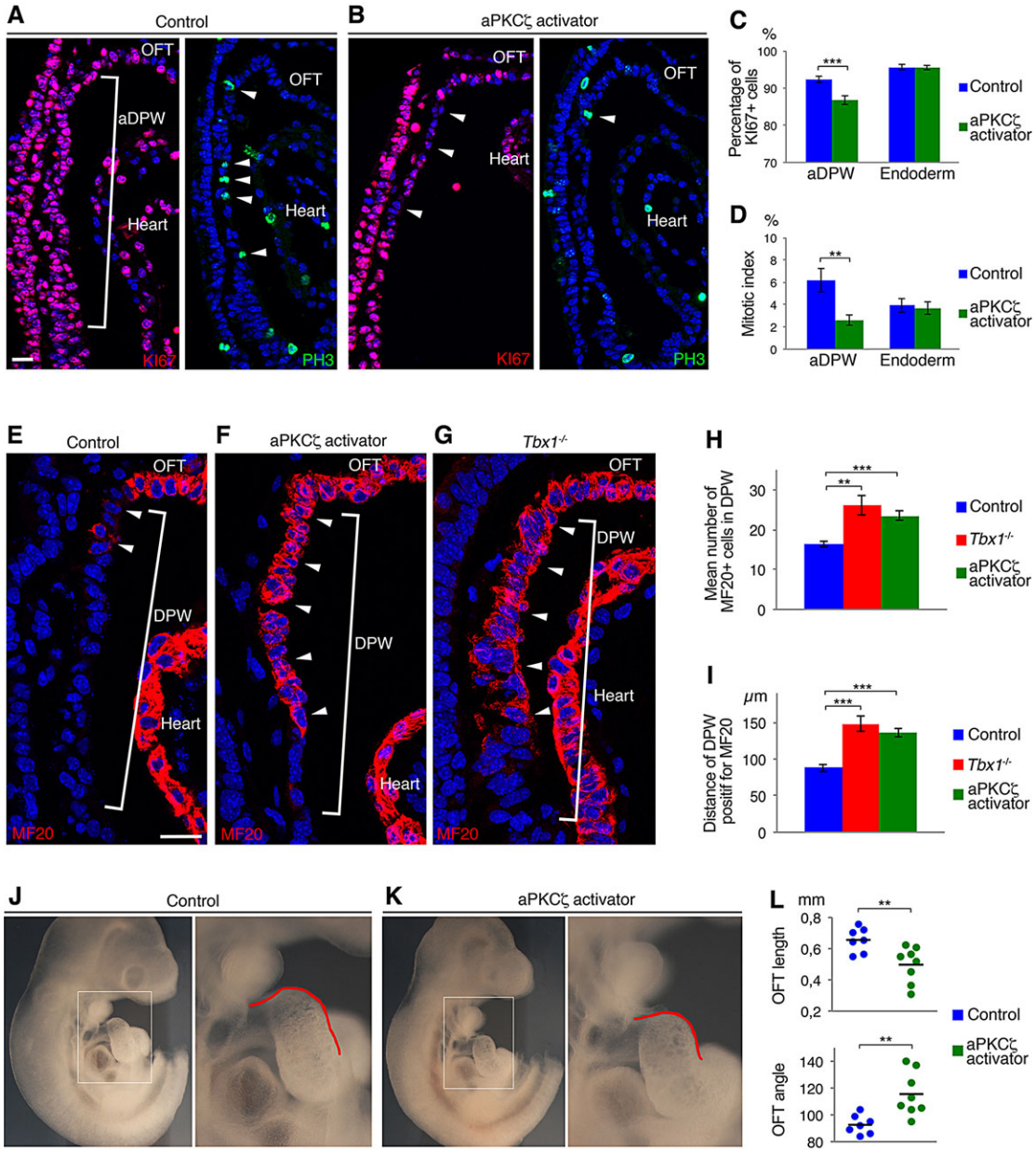

Fig. 8. Activation of aPKCζ reduces proliferation and enhances ectopic differentiation in the anterior DPW. (A,B) Sagittal section showing Ki67- and PH3-positive cells in the aDPW of control embryos (A, bracket and arrowheads), and Ki67-negative and PH3-positive cells in aPKCζ activator-treated embryos (B, arrowheads). (C,D) Quantification showing fewer Ki67-positive cells and a reduced mitotic index in treated compared with control embryos. Proliferation in the underlying endodermal epithelium is unchanged (n=3 control embryos, 5 treated embryos). (E-G) Sagittal section showing ectopic differentiation in the aDPW of an aPKCζ activator-treated embryo compared with *Tbx1*$^{-/-}$ and control embryos (arrowheads in brackets regions). (H,I) Quantification showing an increased number of differentiated cells and MF20 labeling in the aDPW of treated and *Tbx1*$^{-/-}$ embryos compared with controls (n=5 control embryos, 6 treated embryos, 2 *Tbx1*$^{-/-}$ embryos). (J,K) Right view of E9.5 control and treated embryos. (L) Measurement of OFT length and angle as shown by red lines in J and K (n=8 control embryos, 9 treated embryos). *P<0.05; **P<0.01; ***P<0.001. Error bars in C,D,H,I,L represent s.e.m. Scale bars: A,B,E-G: 20 μm; J,K: 500 μm.

We observed that aPKCζ levels are upregulated in the aDPW of *Tbx1*$^{-/-}$ embryos. aPKC proteins play important roles in the regulation of epithelial polarity, including the regulation of adherens junction formation in *Drosophila* and tight junction formation in mammalian epithelial cell lines (Knust and Bossinger, 2002; Suzuki and Ohno, 2006; Suzuki et al., 2001; Xiao and Liu, 2013). Localized Has/PRKCι at the apical junction of myocardial cells is required for heart morphogenesis in zebrafish (Rohr et al., 2006). In addition, aPKC at the apical membrane and junctions has been shown to maintain the apical domain by restricting basal protein localization during epithelial development in *Drosophila* and *Xenopus* (Chalmers et al., 2005; Hutterer et al., 2004). We found that elevated aPKCζ levels in the DPW of *Tbx1*$^{-/-}$ embryos and on exposure to an activator of aPKCζ are associated with an increased apical/basolateral membrane ratio. Activation of aPKCζ results in filopodial loss as well as differentiation and proliferative defects in the SHF and impaired OFT elongation. This suggests that aPKCζ is a downstream effector of TBX1 function in the SHF. Analysis of aPKCζ transcript distribution by *in situ* hybridization did not reveal a detectable increase in the DPW of *Tbx1*$^{-/-}$ embryos (data not shown). aPKCζ protein levels might be regulated post-transcriptionally, as is the case for TBX1 regulation of SRF (Chen et al., 2009). Alternatively,

Development (2014) 141, 4320-4331 doi:10.1242/dev.115022

the regulation of aPKCζ levels and filopodia formation might be indirect. For example, upstream FGF signaling events are required for polarized localization of aPKC in the early mouse embryo (Saiz et al., 2013). *Wnt5a* has recently been shown to be regulated by TBX1 in the SHF (Chen et al., 2012), and *Wnt5a* mutant embryos display OFT defects, potentially mediated by impaired planar cell polarity and loss of filopodia (Schleiffarth et al., 2007; Sinha et al., 2012). Finally, although mesoderm has been shown to be the crucial site for TBX1 function in SHF development, *Tbx1* is also expressed in pharyngeal endoderm, and a non-cell type autonomous role in cell-shape regulation cannot be discounted.

In conclusion, our analysis of the *Tbx1* phenotype and aPKCζ activation in embryo culture suggests that epithelial and progenitor cell states are tightly linked in the DPW and that the control of cell polarity and shape is a regulatory step in SHF development, perturbation of which might contribute to congenital heart defects.

MATERIALS AND METHODS

Experimental animals

The following mouse lines were used: *Mlc1v-nlacZ*-24 [an *Fgf10* enhancer trap line, also termed *Fgf10-nlacZ* (Kelly et al., 2001)], *Tbx1*$^{+/-}$ (Jerome and Papaioannou, 2001), *Mesp1-Cre* (Saga et al., 1999), *Z/EG* (Novak et al., 2000) and CD1 mice. Mice were genotyped as described previously. Animal care was performed in accordance with national and European law.

Histology and immunofluorescence

Embryos were fixed for 1 h in 4% PFA and embedded in paraffin for immunofluorescence or in OCT and were cryosectioned for phalloidin staining. Immunohistochemistry was carried out using standard procedures. Sections were imaged using a Zeiss AxioImager fluorescent microscope with an Apotome module and a Zeiss LSM 780 confocal microscope. Primary antibodies used are listed in supplementary material Table S1. Fluorescent secondary antibodies were obtained from Jackson and Invitrogen and Phalloidin-TRITC was obtained from Sigma (P1951).

Western blot

The anterior pharyngeal regions from wild-type and *Tbx1*$^{-/-}$ embryos were dissected and pooled prior to protein extraction. Anti-aPKCζ (1:4000) and anti-phospho-aPKCζ (1:100) antibodies were used, with anti-actin antibody as loading control. Protein levels were quantified using ImageJ software (gel module, NIH). Two biological replicates were performed for each experiment.

Slice culture, electroporation and dynamic imaging

A thick transverse slice culture system was adapted from Molyneaux et al. (2001). Embryos were dissected in slice culture medium (Boisset et al., 2011), embedded in medium with low melting-point agarose, and 250 µm transverse slices were cut using a tissue chopper (McIlwain). Slices were transferred to culture medium and imaged using a straight two-photon microscope (Nikon A1R-MP) or an inverted spinning-disk microscope (Roper/Nikon Eclipse TI). *Z*-stacks were captured every 5-10 min for 6-8 h. During acquisition explants were maintained at 37°C in a heated chamber.

For electroporation experiments, embryos were dissected, keeping the yolk sac intact. DNA was prepared at 3 µg/µl, injected into the pericardial cavity and electroporated into the DPW (Itasaki et al., 1999). After electroporation, embryos were cultured in rolling bottles for 3 h (see section on whole-embryo culture method), embedded in agarose, sliced and imaged as described above.

Mesp1-Cre and *Z/EG* (*TgACTB*) mice were used to visualize the entire DPW and the dynamics of basal filopodia. An *EGFP* expression vector *pCX-EGFP-N1* was used to express cytoplasmic GFP in DPW cells. An *EGFP-Utrophin* plasmid was used to visualize actin filament dynamics (a gift from A. LeBivic, IBDM; see Burkel et al., 2007). Quantification of filopodia length and lifetime was performed using ImageJ software. Data are presented as mean±s.e.m. *P* values were obtained using a bilateral Mann–Whitney test.

Embryo culture

Embryo culture was performed as previously described (Dominguez et al., 2012). Embryos were cultured from E8.5 (7-11 somites) to E9.5 (18-23 somites). Control embryos were cultured with 0.45% chloroform and treated embryos were cultured with 300 µg/ml of phosphatidic acid (Sigma, P9511), a specific physiological aPKCζ activator (Limatola et al., 1994).

Measurements and quantifications

Membrane length was measured using segmented lines on ImageJ. Apical and basolateral membrane length were measured using aPKCζ and Scribble, respectively. Total membrane length was used to calculate the circularity of the cells. Data are presented as mean±s.e.m. *P* values were obtained using a bilateral Mann–Whitney test.

To quantify fibronectin distribution, the number of DPW cells was counted for each transverse section and the incidence of fibronectin labeling on the lateral and/or apical side of cells was scored to obtain the percentage of fibronectin intercalation between epithelial cells.

aPKCζ immunostaining was performed on paraffin transversal sections at different levels on the anteroposterior axis. Images were acquired using a Zeiss LSM 780 confocal microscope with a 63× objective and measurements were obtained using ImageJ. The cytoplasmic intensity was measured in polygonal areas and the apical membrane intensity was measured on segmented lines along aPKCζ-positive apical membranes. Similar quantification in ventral endodermal cells provided an internal control; a mean intensity ratio was obtained by comparing DPW and endodermal values.

Proliferation in the aDPW and endoderm was quantified on sagittal sections by scoring the percentage of Ki67- and PH3-positive cells. Data were based on at least three sections from three or more embryos. Differentiation in the DPW was quantified relative to a reference point in the distal OFT. The number of MF20-positive cells in the DPW and the extent of differentiated tissue were measured. Right lateral views of whole embryos were used to measure OFT length and the angle between distal and proximal regions using ImageJ. Data are presented as mean±s.e.m. *P* values were obtained using a bilateral Mann–Whitney test.

Acknowledgements

We are grateful to our colleagues in the Kelly group for helpful discussions, to André Le Bivic for discussions and for the *Utrophin-GFP* plasmid and anti-Crumbs3 and anti-PatJ antibodies, and to the IBDM Electron Microscopy service. We acknowledge the France-BioImaging/PICsL infrastructure [ANR-10-INSB-04-01].

Competing interests

The authors declare no competing financial interests.

Author contributions

A.F., K.M. and R.G.K. designed the experiments; A.F., E.S.M. and K.M. performed experiments; A.F., E.S.M., K.M. and R.G.K. analyzed experimental data; and A.F. and R.G.K. wrote the paper.

Funding

This work was supported by the Fondation pour la Recherche Médicale [DEQ20110421300] and the EU-FP7 CP CardioGeNet [Health-2007-B-223463].

Supplementary material

Supplementary material available online at
http://dev.biologists.org/lookup/suppl/doi:10.1242/dev.115022/-/DC1

References

Boisset, J.-C., Andrieu-Soler, C., van Cappellen, W. A., Clapes, T. and Robin, C. (2011). Ex vivo time-lapse confocal imaging of the mouse embryo aorta. *Nat. Protoc.* **6**, 1792-1805.

Burkel, B. M., von Dassow, G. and Bement, W. M. (2007). Versatile fluorescent probes for actin filaments based on the actin-binding domain of utrophin. *Cell Motil. Cytoskeleton* **64**, 822-832.

Cai, C.-L., Liang, X., Shi, Y., Chu, P.-H., Pfaff, S. L., Chen, J. and Evans, S. (2003). Isl1 identifies a cardiac progenitor population that proliferates prior to differentiation and contributes a majority of cells to the heart. *Dev. Cell* **5**, 877-889.

Chalmers, A. D., Pambos, M., Mason, J., Lang, S., Wylie, C. and Papalopulu, N. (2005). aPKC, Crumbs3 and Lgl2 control apicobasal polarity in early vertebrate development. *Development* **132**, 977-986.

Chen, L., Fulcoli, F. G., Tang, S. and Baldini, A. (2009). Tbx1 regulates proliferation and differentiation of multipotent heart progenitors. *Circ. Res.* **105**, 842-851.
Chen, L., Fulcoli, F. G., Ferrentino, R., Martucciello, S., Illingworth, E. A. and Baldini, A. (2012). Transcriptional control in cardiac progenitors: Tbx1 interacts with the BAF chromatin remodeling complex and regulates Wnt5a. *PLoS Genet.* **8**, e1002571.
Choudhry, P. and Trede, N. S. (2013). DiGeorge syndrome gene tbx1 functions through wnt11r to regulate heart looping and differentiation. *PLoS ONE* **8**, e58145.
Cohen, M., Georgiou, M., Stevenson, N. L., Miodownik, M. and Baum, B. (2010). Dynamic filopodia transmit intermittent Delta-Notch signaling to drive pattern refinement during lateral inhibition. *Dev. Cell* **19**, 78-89.
Cooley, J., Whitaker, S., Sweeney, S., Fraser, S. and Davidson, B. (2011). Cytoskeletal polarity mediates localized induction of the heart progenitor lineage. *Nat. Cell Biol.* **13**, 952-957.
Dominguez, J. N., Meilhac, S. M., Bland, Y. S., Buckingham, M. E. and Brown, N. A. (2012). Asymmetric fate of the posterior part of the second heart field results in unexpected left/right contributions to both poles of the heart. *Circ. Res.* **111**, 1323-1335.
Dyer, L. A. and Kirby, M. L. (2009). The role of secondary heart field in cardiac development. *Dev. Biol.* **336**, 137-144.
El-Hashash, A. H. K., Turcatel, G., Varma, S., Berika, M., Al Alam, D. and Warburton, D. (2012). Eya1 protein phosphatase regulates tight junction formation in lung distal epithelium. *J. Cell Sci.* **125**, 4036-4048.
Hutterer, A., Betschinger, J., Petronczki, M. and Knoblich, J. A. (2004). Sequential roles of Cdc42, Par-6, aPKC, and Lgl in the establishment of epithelial polarity during Drosophila embryogenesis. *Dev. Cell* **6**, 845-854.
Itasaki, N., Bel-Vialar, S. and Krumlauf, R. (1999). 'Shocking' developments in chick embryology: electroporation and in ovo gene expression. *Nat. Cell Biol.* **1**, E203-E207.
Jerome, L. A. and Papaioannou, V. E. (2001). DiGeorge syndrome phenotype in mice mutant for the T-box gene, Tbx1. *Nat. Genet.* **27**, 286-291.
Kelly, R. G. (2012). The second heart field. *Curr. Top. Dev. Biol.* **100**, 33-65.
Kelly, R. G. and Papaioannou, V. E. (2007). Visualization of outflow tract development in the absence of Tbx1 using an FgF10 enhancer trap transgene. *Dev. Dyn.* **236**, 821-828.
Kelly, R. G., Brown, N. A. and Buckingham, M. E. (2001). The arterial pole of the mouse heart forms from Fgf10-expressing cells in pharyngeal mesoderm. *Dev. Cell* **1**, 435-440.
Knust, E. and Bossinger, O. (2002). Composition and formation of intercellular junctions in epithelial cells. *Science* **298**, 1955-1959.
Liao, J., Aggarwal, V. S., Nowotschin, S., Bondarev, A., Lipner, S. and Morrow, B. E. (2008). Identification of downstream genetic pathways of Tbx1 in the second heart field. *Dev. Biol.* **316**, 524-537.
Limatola, C., Schaap, D., Moolenaar, W. H. and van Blitterswijk, W. J. (1994). Phosphatidic acid activation of protein kinase C-zeta overexpressed in COS cells: comparison with other protein kinase C isotypes and other acidic lipids. *Biochem. J.* **304**, 1001-1008.
Linask, K. K. (1992). N-cadherin localization in early heart development and polar expression of Na^+, K^+-ATPase, and integrin during pericardial coelom formation and epithelialization of the differentiating myocardium. *Dev. Biol.* **151**, 213-224.
Linask, K. K., Manisastry, S. and Han, M. (2005). Cross talk between cell-cell and cell-matrix adhesion signaling pathways during heart organogenesis: implications for cardiac birth defects. *Microsc. Microanal.* **11**, 200-208.
Martín-Blanco, E. and Knust, E. (2001). Epithelial morphogenesis: filopodia at work. *Curr. Biol.* **11**, R28-R31.
Mjaatvedt, C. H., Nakaoka, T., Moreno-Rodriguez, R., Norris, R. A., Kern, M. J., Eisenberg, C. A., Turner, D. and Markwald, R. R. (2001). The outflow tract of the heart is recruited from a novel heart-forming field. *Dev. Biol.* **238**, 97-109.
Molyneaux, K. A., Stallock, J., Schaible, K. and Wylie, C. (2001). Time-lapse analysis of living mouse germ cell migration. *Dev. Biol.* **240**, 488-498.
Novak, A., Guo, C., Yang, W., Nagy, A. and Lobe, C. G. (2000). Z/EG, a double reporter mouse line that expresses enhanced green fluorescent protein upon Cre-mediated excision. *Genesis* **28**, 147-155.
Pane, L. S., Zhang, Z., Ferrentino, R., Huynh, T., Cutillo, L. and Baldini, A. (2012). Tbx1 is a negative modulator of Mef2c. *Hum. Mol. Genet.* **21**, 2485-2496.
Papangeli, I. and Scambler, P. (2013). The 22q11 deletion: DiGeorge and velocardiofacial syndromes and the role of TBX1. *Wiley Interdiscip. Rev. Dev. Biol.* **2**, 393-403.
Rochais, F., Mesbah, K. and Kelly, R. G. (2009). Signaling pathways controlling second heart field development. *Circ. Res.* **104**, 933-942.
Rohr, S., Bit-Avragim, N. and Abdelilah-Seyfried, S. (2006). Heart and soul/PRKCi and nagie oko/Mpp5 regulate myocardial coherence and remodeling during cardiac morphogenesis. *Development* **133**, 107-115.
Saga, Y., Miyagawa-Tomita, S., Takagi, A., Kitajima, S., Miyazaki, J. and Inoue, T. (1999). MesP1 is expressed in the heart precursor cells and required for the formation of a single heart tube. *Development* **126**, 3437-3447.
Saiz, N., Grabarek, J. B., Sabherwal, N., Papalopulu, N. and Plusa, B. (2013). Atypical protein kinase C couples cell sorting with primitive endoderm maturation in the mouse blastocyst. *Development* **140**, 4311-4322.
Sanders, T. A., Llagostera, E. and Barna, M. (2013). Specialized filopodia direct long-range transport of SHH during vertebrate tissue patterning. *Nature* **497**, 628-632.
Schleiffarth, J. R., Person, A. D., Martinsen, B. J., Sukovich, D. J., Neumann, A., Baker, C. V. H., Lohr, J. L., Cornfield, D. N., Ekker, S. C. and Petryk, A. (2007). Wnt5a is required for cardiac outflow tract septation in mice. *Pediatr. Res.* **61**, 386-391.
Shibue, T., Brooks, M. W., Inan, M. F., Reinhardt, F. and Weinberg, R. A. (2012). The outgrowth of micrometastases is enabled by the formation of filopodium-like protrusions. *Cancer Discov.* **2**, 706-721.
Sinha, T., Wang, B., Evans, S., Wynshaw-Boris, A. and Wang, J. (2012). Disheveled mediated planar cell polarity signaling is required in the second heart field lineage for outflow tract morphogenesis. *Dev. Biol.* **370**, 135-144.
Suzuki, A. and Ohno, S. (2006). The PAR-aPKC system: lessons in polarity. *J. Cell Sci.* **119**, 979-987.
Suzuki, A., Yamanaka, T., Hirose, T., Manabe, N., Mizuno, K., Shimizu, M., Akimoto, K., Izumi, Y., Ohnishi, T. and Ohno, S. (2001). Atypical protein kinase C is involved in the evolutionarily conserved par protein complex and plays a critical role in establishing epithelia-specific junctional structures. *J. Cell Biol.* **152**, 1183-1196.
Thiery, J. P., Acloque, H., Huang, R. Y. J. and Nieto, M. A. (2009). Epithelial-mesenchymal transitions in development and disease. *Cell* **139**, 871-890.
Trinh, L. A. and Stainier, D. Y. R. (2004). Fibronectin regulates epithelial organization during myocardial migration in zebrafish. *Dev. Cell* **6**, 371-382.
Trinh, L. A., Yelon, D. and Stainier, D. Y. R. (2005). Hand2 regulates epithelial formation during myocardial diferentiation. *Curr. Biol.* **15**, 441-446.
van Bueren, K. L., Papangeli, I., Rochais, F., Pearce, K., Roberts, C., Calmont, A., Szumska, D., Kelly, R. G., Bhattacharya, S. and Scambler, P. J. (2010). Hes1 expression is reduced in Tbx1 null cells and is required for the development of structures affected in 22q11 deletion syndrome. *Dev. Biol.* **340**, 369-380.
Vincent, S. D. and Buckingham, M. E. (2010). How to make a heart: the origin and regulation of cardiac progenitor cells. *Organogenesis Dev.* **90**, 1-41.
Virágh, S. and Challice, C. E. (1973). Origin and differentiation of cardiac muscle cells in the mouse. *J. Ultrastruct. Res.* **42**, 1-24.
Vitelli, F., Taddei, I., Morishima, M., Meyers, E. N., Lindsay, E. A. and Baldini, A. (2002). A genetic link between Tbx1 and fibroblast growth factor signaling. *Development* **129**, 4605-4611.
Waldo, K. L., Kumiski, D. H., Wallis, K. T., Stadt, H. A., Hutson, M. R., Platt, D. H. and Kirby, M. L. (2001). Conotruncal myocardium arises from a secondary heart field. *Development* **128**, 3179-3188.
Xiao, H. and Liu, M. (2013). Atypical protein kinase C in cell motility. *Cell. Mol. Life Sci.* **70**, 3057-3066.
Xu, H., Morishima, M., Wylie, J. N., Schwartz, R. J., Bruneau, B. G., Lindsay, E. A. and Baldini, A. (2004). Tbx1 has a dual role in the morphogenesis of the cardiac outflow tract. *Development* **131**, 3217-3227.
Zhang, Z., Huynh, T. and Baldini, A. (2006). Mesodermal expression of Tbx1 is necessary and sufficient for pharyngeal arch and cardiac outflow tract development. *Development* **133**, 3587-3595.

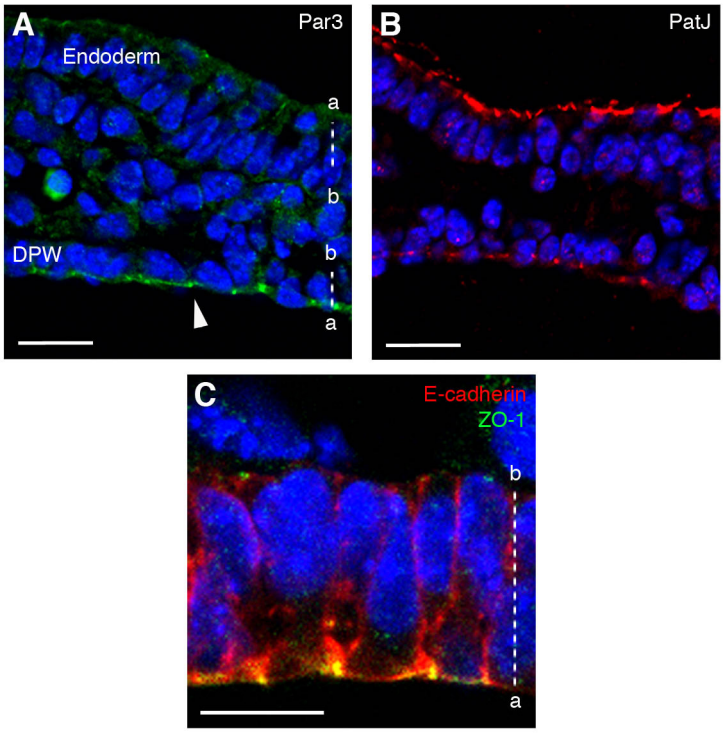

Fig. S1. **Epithelial markers in the dorsal pericardial wall**. (**A**,**B**) Par3 and PatJ accumulate at apical junctions in DPW cells and pharyngeal endoderm at E9.5. (**C**) High magnification view of endodermal cells showing localization of ZO-1 at apical junctions and E-cadherin accumulation at apical junctions and along the lateral membrane (compare with Fig. 1L). The apical (a) and basal (b) sides of cells in pharyngeal endoderm and the dorsal pericardial wall are indicated by broken lines in A and C. Scale bars: A,B: 20μm; C,D: 10μm.

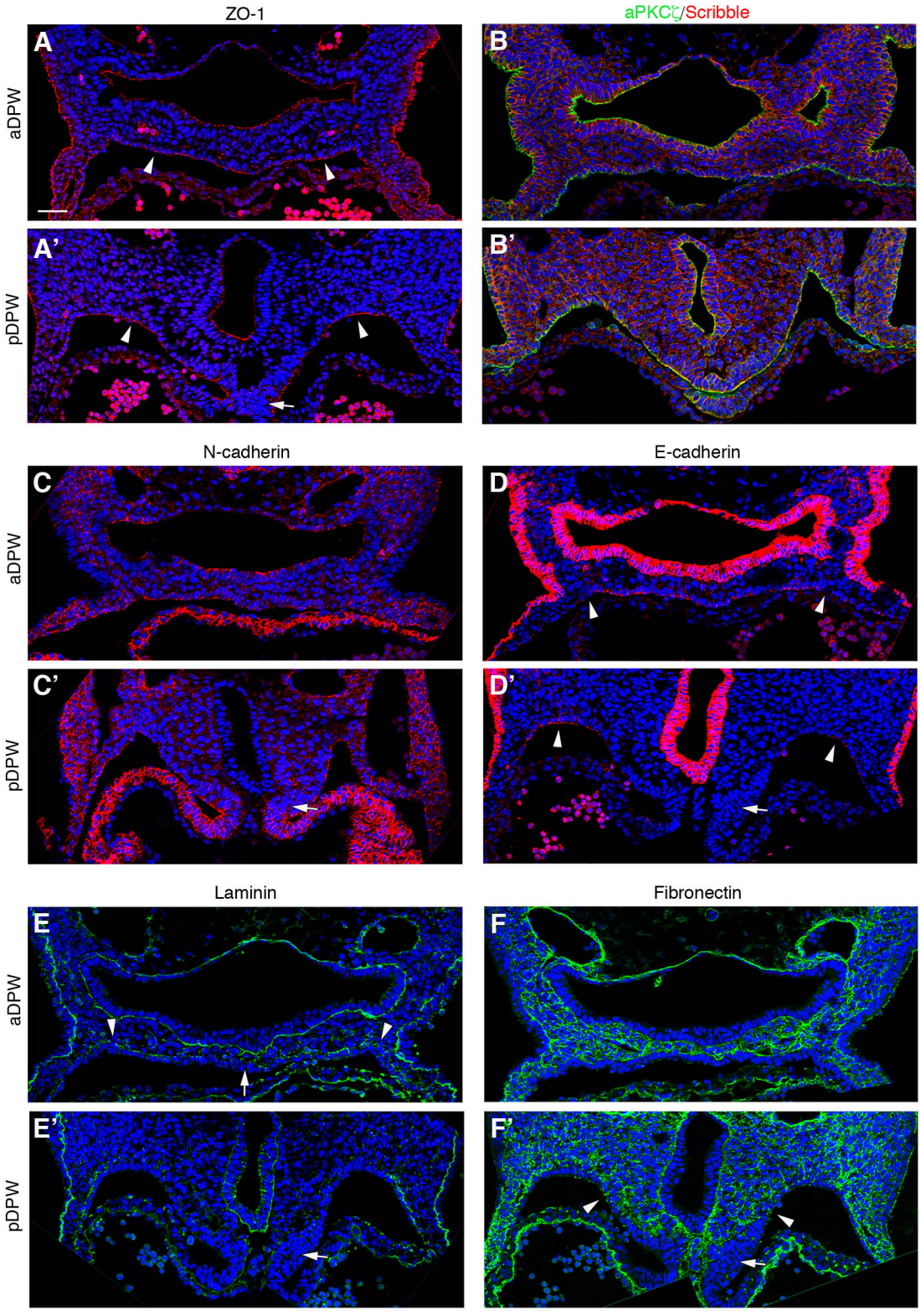

Fig. S2. Spatial heterogeneity in the epithelial properties of the dorsal percicardial wall. Immunofluorescence labeling of transverse sections at E9.5 in the aDPW and pDPW. (**A-C'**) ZO-1, aPKCζ, Scribble and N-cadherin accumulate throughout the entire DPW. E-cadherin accumulates in broad bilateral populations of cells in the aDPW (**D** arrowheads), but is restricted to lateral regions of the pDPW (**D'** arrowheads). (**E**) Laminin staining reveals an

irregular basal lamina in the aDPW with medial (arrow) and lateral gaps (arrowheads); and is restricted to the lateral regions of the pDPW (**E'**). Fibronectin is not observed between epithelial cells in the aDPW (**F**), and is occasionally observed between epithelial cells in the pDPW (**F'** arrowheads). Arrows in A',C',D',E' and F' show a condensed group of mesenchymal cells close to the venous pole of the heart. Scale bars: 30μm.

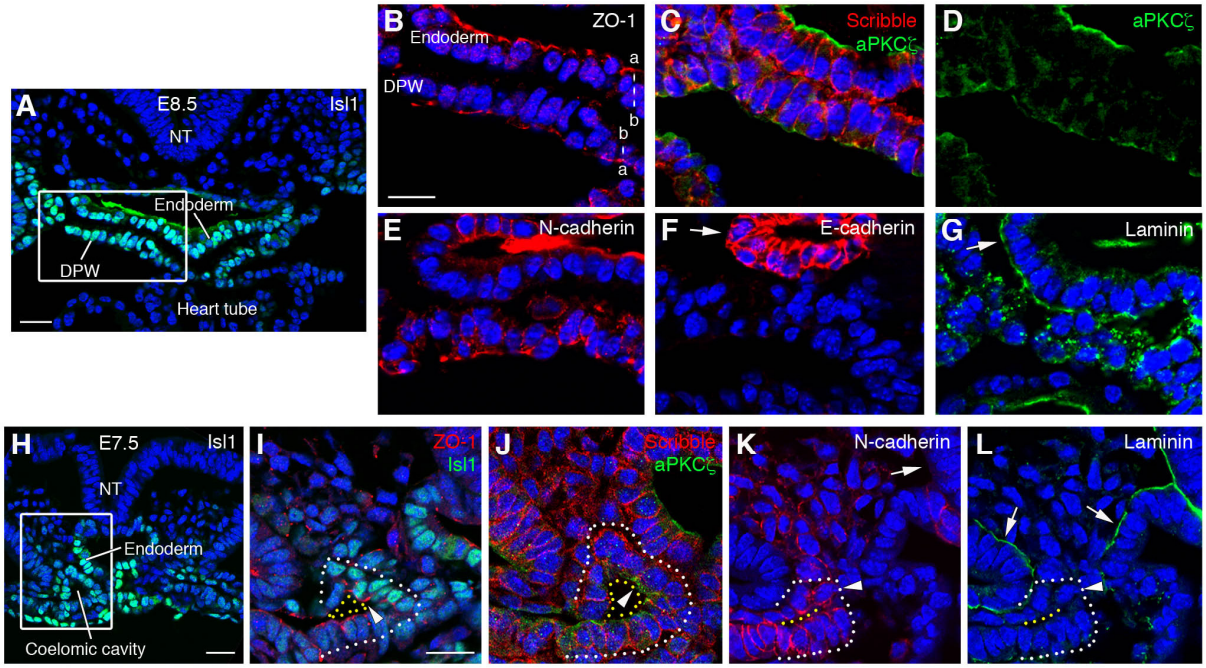

Fig. S3. Temporal maturation of epithelial properties in the dorsal pericardial wall. Immunofluorescence labeling on transverse sections of E8.5 and E7.5 embryos (A-G). (**A**) ISL1 expression at E8.5; the region shown in B-G is boxed. (**B**) ZO-1 accumulates on the apical junctions of DPW cells. (**C,D**) aPKCζ accumulates on the apical membrane and Scribble on the basolateral membrane. (**E,F**) N-cadherin accumulates on the apical side whereas E-cadherin is not expressed in the DPW although is present in the endoderm (arrow). (**G**) Laminin is punctuated and the basal lamina of the DPW disorganized compared to the endoderm (arrow). Immunofluorescence labeling on transverse sections of E7.5 embryos (H-L). (**H**) ISL1 expression at E7.5; the region shown in I-L is boxed. (**I**) ZO-1 is localized on the apical side of coelomic epithelial cells (arrowhead). (**J**) aPKCζ and Scribble distinguish apical (arrowhead) and basolateral membrane domains. (**K**) N-cadherin accumulates around the

membrane of coelomic epithelial cells (arrowhead). (**L**) Laminin is absent on the basal side of coelomic epithelial cells (arrowhead), in contrast to endoderm and ectoderm (arrows). White dotted lines delimit the basal side of the coelomic epithelial layer, and yellow dotted lines the apical side. NT: neural tube. Scale bars: A,H: 30 µm ; B-G,I-L: 20µm.

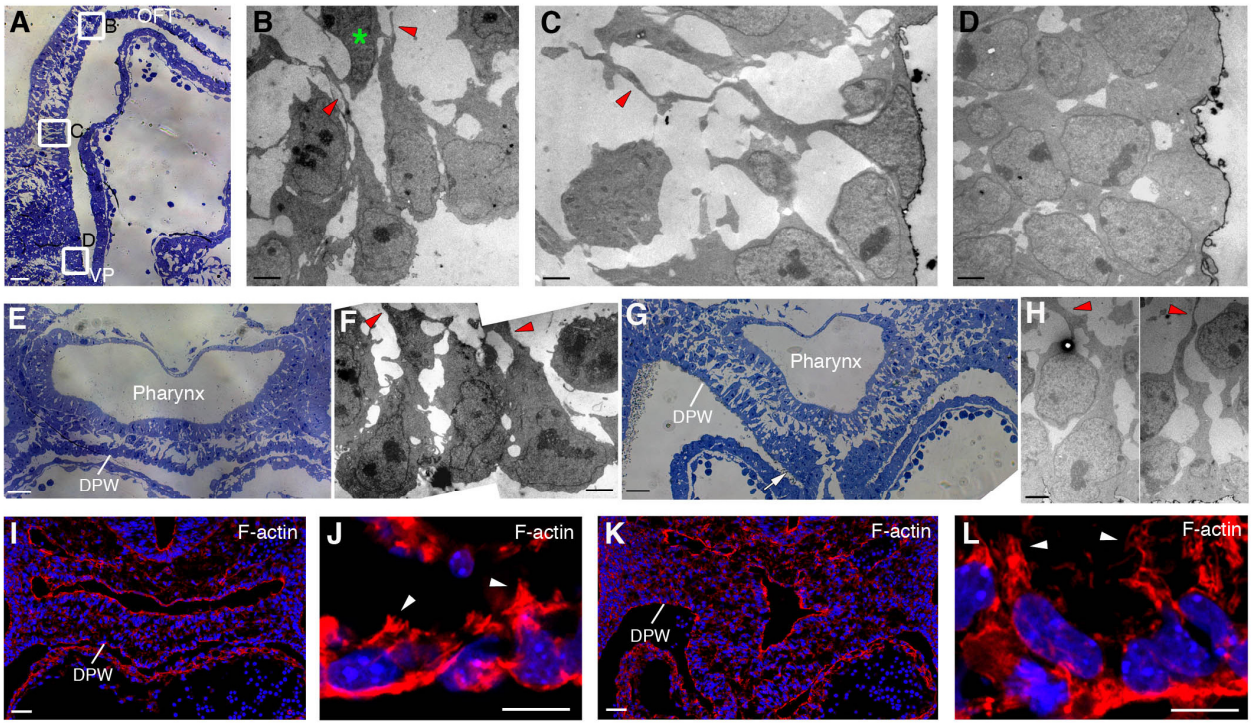

Fig. S4. Basal filopodia in the dorsal pericardial wall. (**A**) Sagital section of an E9.5 embryo showing three regions between the outflow tract and venous pole of the heart (boxes B, C and D correspond to panels B, C and D). Transmission electron microscopy shows basal protrusions in the anterior (**B**, arrowheads, green asterisk indicates filopodial contact with an overlying mesenchymal cell) and middle regions (**C**, arrowheads). Condensed mesenchymal cells close to the venous pole of the heart are shown in **D** (corresponding to the region indicated by an arrow in G). Basal protrusions are visible on transverse sections in the aDPW (**E, F** arrowheads) and pDPW (**G, H** arrowheads). Basal actin filaments are present in aDPW (**I, J** arrowheads) and pDPW (**K, L** arrowheads). Scale bars: A,E,G,I,K: 30 µm; B-D,F,H: 2µm; J,L: 10µm.

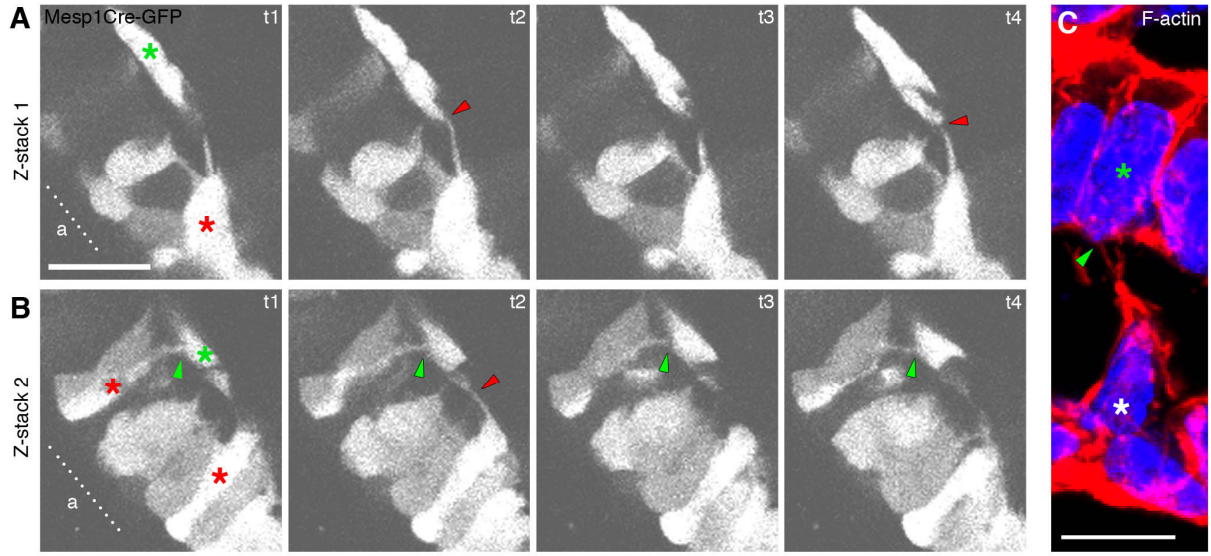

Fig. S5. Basal filopodia in cells in the DPW contact overlying mesenchymal and pharyngeal endodermal cells. (**A,B**) Images extracted from a time-lapse movie using a *Mesp1-Cre-GFP* embryo showing filopodia from DPW cells (red asterisk) contacting an overlying Mesp1-Cre lineage labeled mesenchymal cell (green asterisk) with transient (red arrowheads) and stable contacts (green arrowheads). (**C**) Transverse section after phalloidin staining showing actin filament containing filopodia (arrowhead) in a DPW cell (white asterisk) contacting an overlying endodermal cell (green asterisk). Scale bars: 10μm.

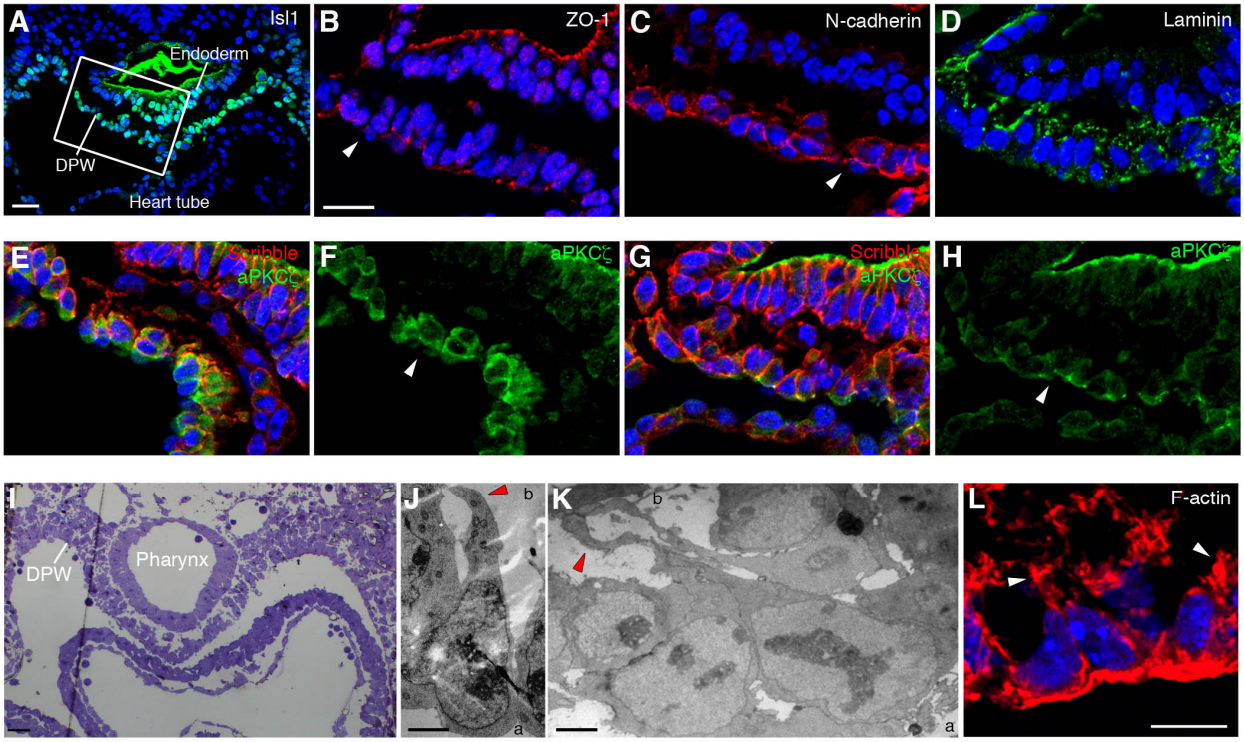

Fig. S6. Epithelial markers in E8.5 *Tbx1*$^{-/-}$ embryos and filopodia in the posterior dorsal pericardial wall of *Tbx1*$^{-/-}$embryos. (**A**) Transverse section of an E8.5 *Tbx1*$^{-/-}$ embryo showing ISL1 expression in the DPW; the boxed region corresponds to that shown in panels B-H. Nuclei can be observed on the coelomic side of the ZO-1 (**B**) and N-cadherin (**C**) labelled apical membrane (arrowheads). N-cadherin also accumulates on the lateral membrane (compare to Fig. S3E). (**D**) Laminin staining is punctuated. The intensity of aPKCζ labeling is stronger in the most anterior region of the DPW (**E,F**) but not more posteriorly (**G,H**). (**I**) Transverse section of an E9.5 *Tbx1*$^{-/-}$ embryo at the level of the pDPW. (**J,K**) Transmission electron microscopy showing basal protrusions in cells in the *Tbx1*$^{-/-}$ pDPW (arrowheads). (**L**) Phalloidine staining showing the presence of basal actin filaments in the pDPW (arrowheads). Scale bars: A,I: 30μm; B-H: 20μm; J,K: 2μm; L: 10μm.

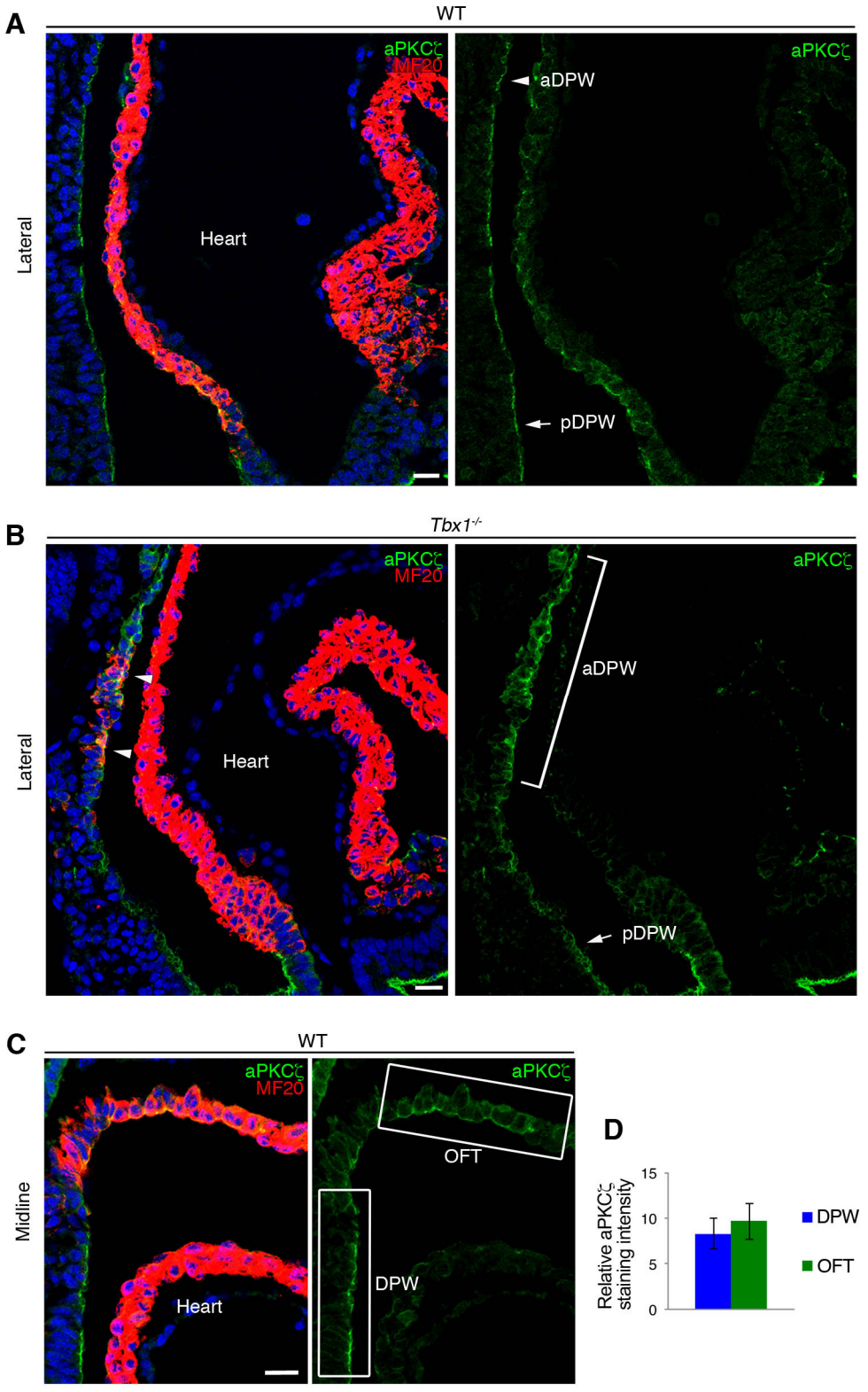

Fig. S7. Differentiation in the outflow tract and dorsal pericardial wall. (**A**) Lateral sagittal section of E9.5 wildtype embryo showing equivalent aPKCζ expression in the aDPW (arrowhead) and pDPW (arrow) and no MF20 positive cells in the DPW. (**B**) Lateral sagittal section of a *Tbx1*$^{-/-}$ embryo showing an increase in aPKCζ labeling in the aDPW (right arrowheads) compared to the pDPW (right arrow) and ectopically differentiated MF20

positive cells in the DPW (left arrowheads). (**C**) Sagittal section through the midline of an E9.5 wildtype embryo showing differentiated MF20 positive cells in the distal outflow tract. (**D**) Quantification reveals that the total relative aPKCζ staining intensity in epithelial cells of the DPW and outflow tract (as show in boxes in C) is unchanged. Quantification in D was based on multiple sections from four embryos. Scale bars: 20μm.

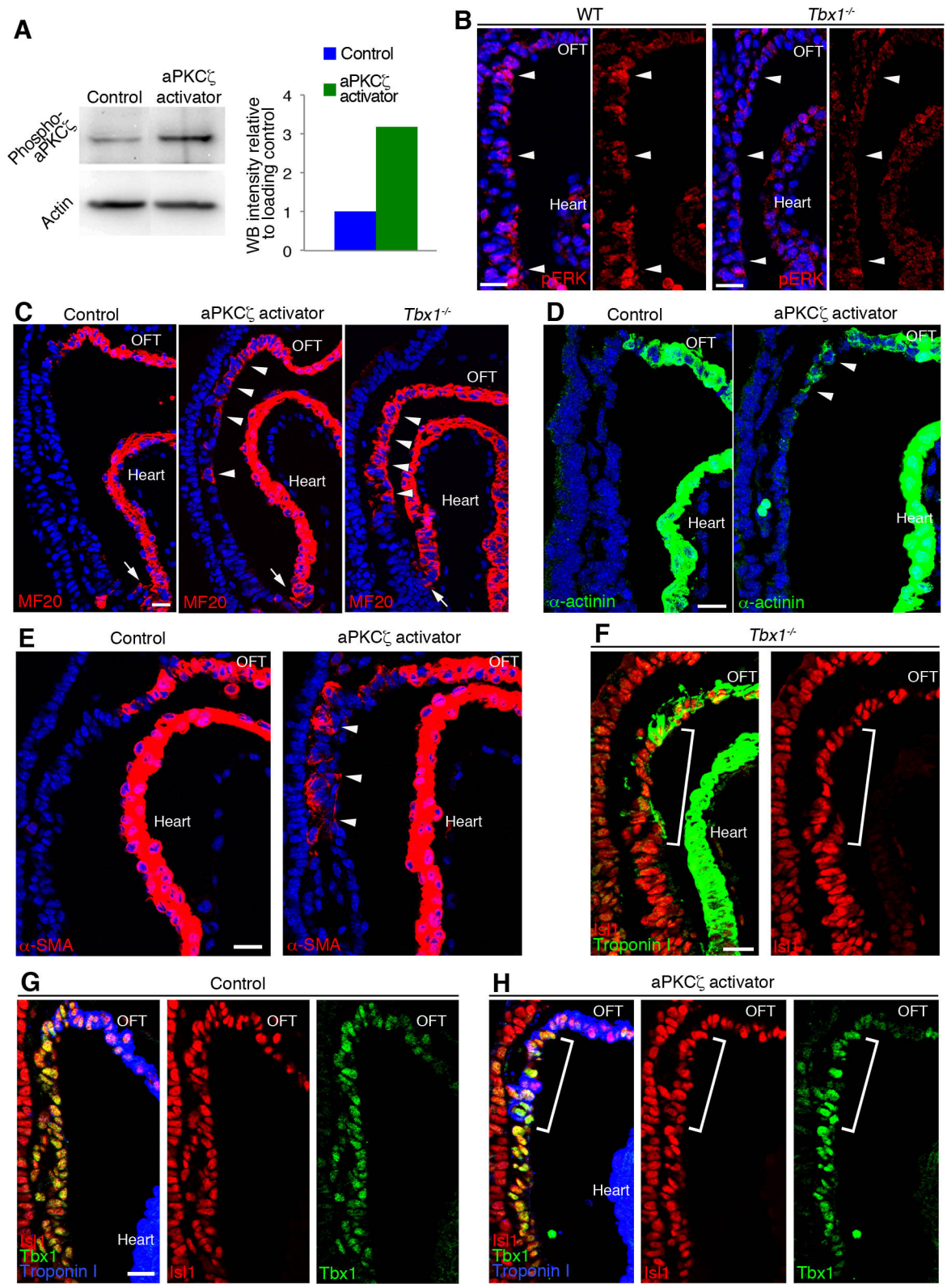

Fig. S8. Protein expression in the dorsal pericardial wall of *Tbx1*$^{-/-}$ embryos and on aPKCζ activation. (**A**) Western blot and intensity quantification for extracts prepared from the pharyngeal region of control and aPKCζ activator treated embryos showing an increase in phosphorylated aPKCζ protein levels in treated embryos. (**B**) Sagittal sections showing reduced phosphoERK expression in the aDPW of a *Tbx1*$^{-/-}$ embryo compared to wildtype

(arrowheads). (**C**) Sagittal sections showing ectopic expression of MF20 in the aDPW of aPKCζ activator treated and *Tbx1*$^{-/-}$ embryos (arrowheads), but not at the venous pole (arrows), compared to a control embryo. Sections showing ectopic expression (arrowheads) of α-actinin **(D)** and α-SMA **(E)** in treated compared to control embryos. (**F**) Ectopic expression of Troponin I in the aDPW of a *Tbx1*$^{-/-}$ embryo (brackets); note that cells maintain ISL1 expression. (**G,H**) Ectopic expression (brackets) of Troponin I in the aDPW of aPKCζ activator treated (H) compared to control (G) embryos; note that cells maintain ISL1 and TBX1 expression. Scale bars: 20μm.

Supplementary Table 1: Primary antibodies

β-galactosidase	Rabbit	1/300	MP Biomedicals 0855976
β-galactosidase	Mouse	1/200	Promega Z378A
Islet1	Mouse	1/100	DSHB 394D05 and 402D06
ZO-1	Rabbit	1/200	Invitrogen 61-7300
Par3	Rabbit	1/200	Millipore 07-330
aPKC-ζ	Rabbit	1/200	Santa Cruz sc-216
Phospho-aPKC-ζ	Rabbit	1/100	Santa Cruz sc-101778 (Trh410)
Crumbs3	Rabbit	1/100	Gift from A. LeBivic, IBDM
PatJ	Rabbit	1/100	Gift from A. LeBivic, IBDM
Laminin 1-2	Rabbit	1/1000	Novus Biologicals NB300-144
Fibronectin	Rabbit	1/100	Abcam ab2413
N-cadherin	Mouse	1/200	Invitrogen 33-3900
E-cadherin	Mouse	1/200	BD Transduction Laboratories 610181
α-Tubulin	Mouse	1/500	Sigma T9026
β-catenin	Rabbit	1/100	Abcam ab2365
Tbx1	Rabbit	1/100	LifeSpan Biosciences LS-C31179/7296
Acetylated **α**-Tubulin	Mouse	1/500	Sigma T7451
Scribble	Goat	1/200	Santa Cruz sc-11049
MF20 sarcomeric myosin heavy chain	Mouse	1/50	DSHB MF20
Actin	Mouse	1/2000	Sigma A3853
Phospho-ERK	Rabbit	1/100	Cell signaling p44/42 MAPK 4376
KI67	Rat	1/25	Dako M7249
Phospho Histone H3	Rabbit	1/400	Upstate cell signaling 06-570
α-Actinin	Mouse	1/500	Sigma A7811
α-SMA	Mouse	1/500	Sigma F3777
Troponin I	Goat	1/100	Abcam ab56357
Phospho-Tyrosine	Mouse	1/100	Millipore 05-1050

Movie 1. Time-lapse imaging of an E8.5 *Mesp1-Cre* GFP wildtype embryo showing dynamic basal filopodia. a and b show apical and basal sides. Image acquired every 5 minutes over 230 minutes of culture.

Movie 2. Time-lapse imaging of E8.5 control (left) and *Tbx1*$^{-/-}$ (right) embryos showing dynamic basal actin filaments in Utrophin-GFP electroporated cells. a and b show apical and basal sides. Image acquired every 5 minutes over 320 (left) and 205 (right) minutes of culture.

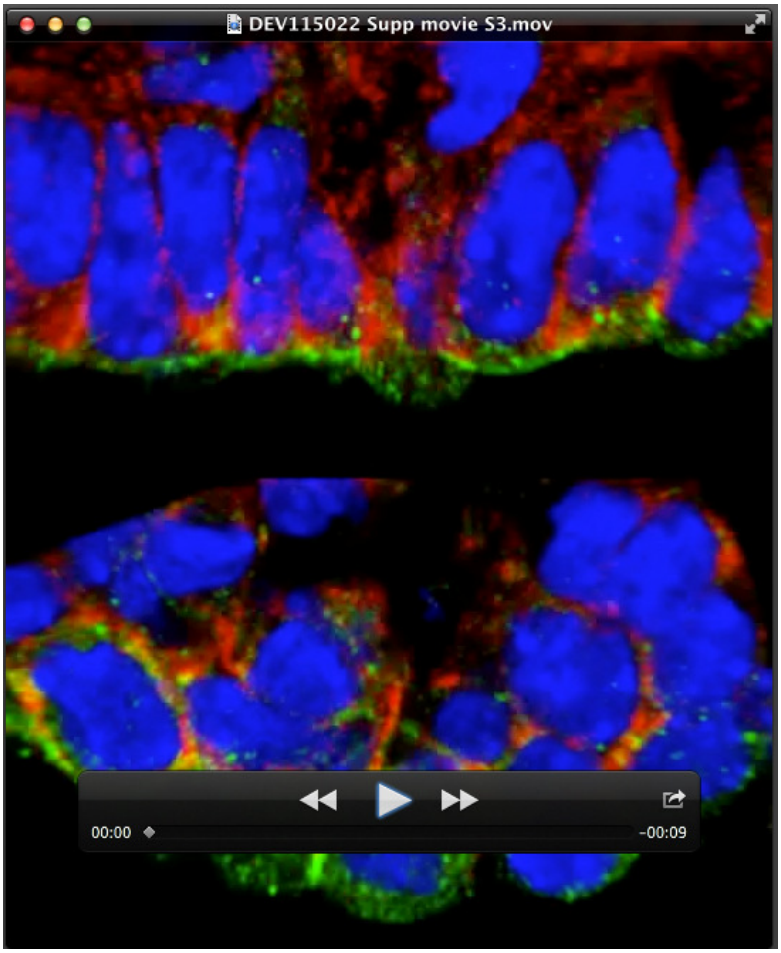

Movie 3. aPKCζ localises to the apical membrane of cells in the dorsal pericardial wall. Apical is to the bottom and basal to the top. Wildtype DPW cells are elongated, basolateral membranes are stained by Scribble (red), whereas aPKCζ (green) accumulates on the apical membrane (top movie). Cells in the DPW of *Tbx1*$^{-/-}$ embryos are rounder, with an enlarged apical membrane labeled by aPKCζ (bottom movie).

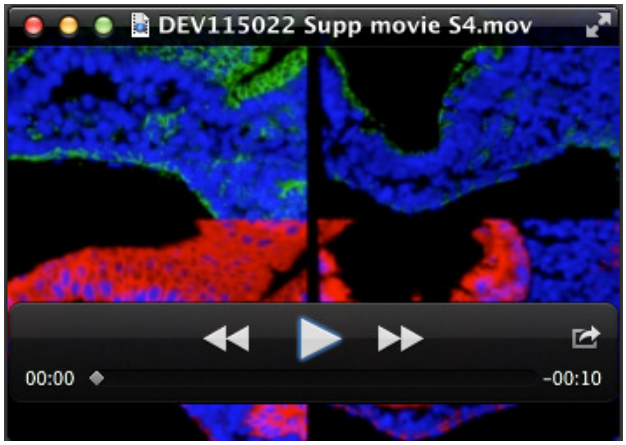

Movie 4. ZO-1 and E-cadherin localization in the dorsal pericardial wall. 3D reconstruction of ZO-1 (green) and E-cadherin (red) in wildtype (left) and *Tbx1*$^{-/-}$ (right) E9.5 embryos. ZO-1 and E-cadherin co-localize on the apical side of the nucleus in wildtype cells (left, arrowheads). In *Tbx1*$^{-/-}$ embryos, nuclei are observed on the coelomic side of ZO-1 and E-cadherin labeling (right, arrowheads).

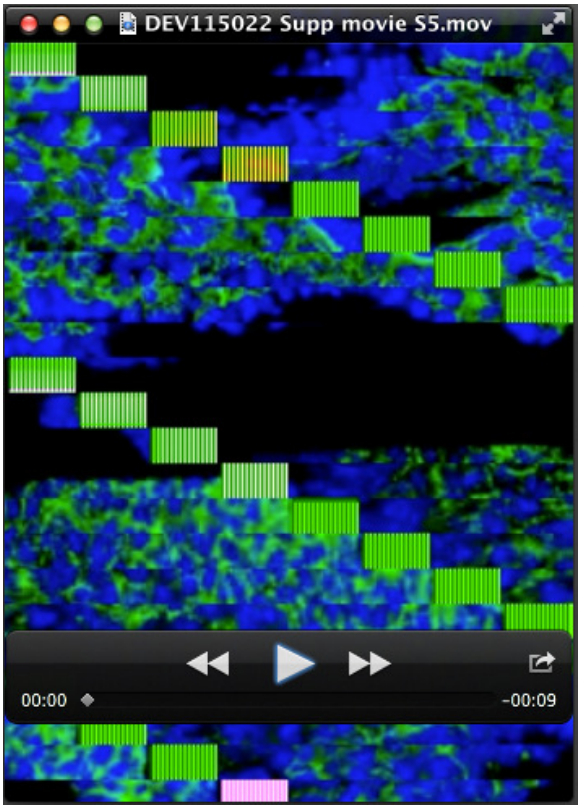

Movie 5. Fibronectin mislocalization in the dorsal pericardial wall of *Tbx1*$^{-/-}$ embryos. In wildtype embryos the DPW epithelium (top, arrowhead) is free of Fibronectin protein (green); while Fibronectin is observed between cells in the epithelium of *Tbx1*$^{-/-}$ embryos (bottom).

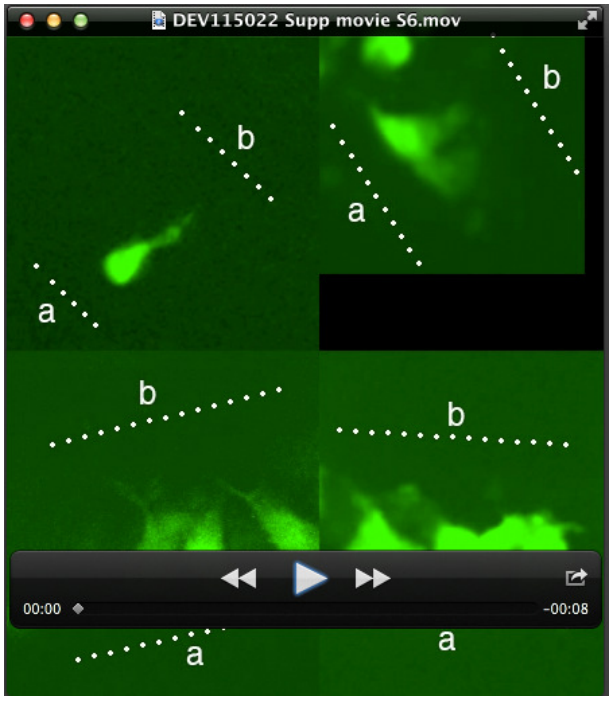

Movie 6. Time-lapse imaging of E8.5 control (top and bottom left) and *Tbx1*$^{-/-}$ (top and bottom right) embryos showing dynamic basal filopodia in eGFP electroporated cells. a and b show apical and basal sides. Top: image acquired every 5 minutes over 220 minutes of culture. Bottom left: image acquired every 7.5 minutes over 330 minutes culture. Bottom right: image acquired every 5 minutes over 120 minutes.